

A UNIFORM MEASUREMENT OF THE GALACTIC ABUNDANCE GRADIENT

by

JOHN R DONOR III

Bachelor of Arts, 2014  
Austin College  
Sherman, TX

Submitted to the Graduate Faculty of the  
College of Science and Engineering  
Texas Christian University  
in partial fulfillment of the requirements  
for the degree of

Master of Science

December 2017

A UNIFORM MEASUREMENT OF THE GALACTIC ABUNDANCE GRADIENT

by

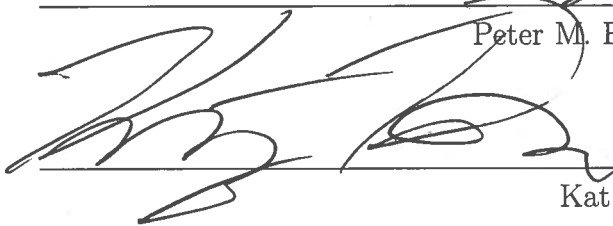
John R Donor III

Dissertation Approved:



---

Peter M. Frinchaboy III



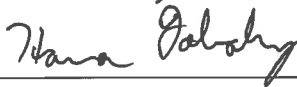
---

Kat Barger



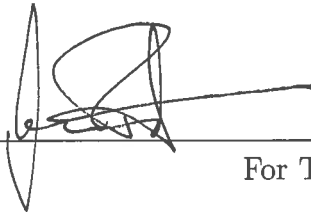
---

Doug Ingram



---

Hana Dobrovolny



---

For The College of Science and Engineering



## ACKNOWLEDGEMENTS

This material is based upon work supported by the National Science Foundation under award AST-1311835 and AST-1715662 to P.M.F.

This research made use of Astropy, a community-developed core Python package for Astronomy (Astropy Collaboration, 2013).

This publication makes use of data products from the Two Micron All Sky Survey, which is a joint project of the University of Massachusetts and the Infrared Processing and Analysis Center/California Institute of Technology, funded by the National Aeronautics and Space Administration and the National Science Foundation.

This publication makes use of data products from the Wide-field Infrared Survey Explorer, which is a joint project of the University of California, Los Angeles, and the Jet Propulsion Laboratory/California Institute of Technology, funded by the National Aeronautics and Space Administration.

Funding for the Sloan Digital Sky Survey IV has been provided by the Alfred P. Sloan Foundation, the U.S. Department of Energy Office of Science, and the Participating Institutions. SDSS acknowledges support and resources from the Center for High-Performance Computing at the University of Utah. The SDSS web site is [www.sdss.org](http://www.sdss.org).

SDSS is managed by the Astrophysical Research Consortium for the Participating Institutions of the SDSS Collaboration including the Brazilian Participation Group, the Carnegie Institution for Science, Carnegie Mellon University, the Chilean Participation Group, the French Participation Group, Harvard-Smithsonian Center for Astrophysics, Instituto de Astrofísica de Canarias, The Johns Hopkins University, Kavli Institute for the Physics and Mathematics of the Universe (IPMU) / University of Tokyo, Lawrence Berkeley National Laboratory, Leibniz Institut für Astrophysik Potsdam (AIP), Max-Planck-Institut für Astronomie (MPIA Heidelberg), Max-Planck-Institut für Astrophysik (MPA Garching), Max-Planck-Institut für Extraterrestrische Physik (MPE), National Astronomical Observatories of China, New Mexico State University, New York University, University of Notre Dame, Observatorio Nacional / MCTI, The Ohio State University, Pennsylvania State University, Shanghai Astronomical Observatory, United Kingdom Participation Group, Universidad Nacional Autónoma de México, University of Arizona, University of Colorado Boulder, University of Oxford, University of Portsmouth, University of Utah, University of Virginia, University of Washington, University of Wisconsin, Vanderbilt University, and Yale University.

# Contents

<b>1</b>	<b>General Scientific Introduction</b>	<b>1</b>
1.1	Astronomical Measurements . . . . .	1
1.1.1	The Magnitude System . . . . .	1
1.1.2	Distance . . . . .	2
1.1.3	Photometry . . . . .	4
1.1.4	Effects of Interstellar Dust . . . . .	6
1.2	Spectroscopy Basics . . . . .	8
1.2.1	Spectral Lines and Doppler Shift . . . . .	8
1.2.2	Metallicity . . . . .	9
1.3	Star Clusters . . . . .	10
1.4	Stellar Evolution . . . . .	11
1.5	Isochrones . . . . .	13
1.5.1	Isochrone Fitting . . . . .	14
<b>2</b>	<b>Objectives</b>	<b>16</b>
<b>3</b>	<b>Chemical Evolution of the Galactic Disk</b>	<b>18</b>
3.1	Galactic Structure . . . . .	18
3.2	Galactic Chemical Evolution Models . . . . .	19
3.3	Recent Work . . . . .	22
3.3.1	Variation with Location and Age . . . . .	24
3.3.2	The Open Cluster Chemical Abundance and Mapping (OCCAM) Survey . . . . .	26
<b>4</b>	<b>The Open Cluster Chemical Abundance &amp; Mapping Survey</b>	<b>27</b>
4.1	The APOGEE Survey . . . . .	27
4.2	Identifying Member Stars in OCCAM Open Clusters . . . . .	29
4.2.1	Likely Member Targeting . . . . .	29
4.2.2	OCCAM Spectroscopic Observed Stars - SDSS DR14 . . . . .	31
4.2.3	OCCAM Observed Membership Criteria . . . . .	33
4.3	Determination of Galactic Abundance Gradients . . . . .	36
4.3.1	Error Analysis . . . . .	37

<b>5</b>	<b>Results &amp; Discussion</b>	<b>38</b>
5.1	Galactic Abundance Gradients . . . . .	38
5.1.1	Is The Thick Disk Real?: The $Z_{GC}$ Divided Sample . . . . .	39
5.1.2	The Gradient Evolution?: The Age Divided Sample . . . . .	41
5.1.3	Discussion . . . . .	44
<b>6</b>	<b>Future Work</b>	<b>46</b>
6.1	Improve Isochrone Fitting . . . . .	46
6.2	The <i>Gaia</i> Survey . . . . .	48
6.3	Improved Z-Height Measurements . . . . .	49
<b>A</b>	<b>The Cluster Sample</b>	<b>50</b>

Vita

Abstract

# List of Figures

1.1	Transmission vs wavelength (in Å) for the 3 2MASS filters (from Rodrigo 1999) . . . . .	4
1.2	Color-Magnitude Diagram (CMD) for cluster NGC 2682 . . . . .	5
1.3	Left: The evolution of an isochrone of constant metallicity over a range of ages in Gyr, Right: a sample of 1 Gyr isochrones spanning a range of metallicities [Fe/H] (see below). Both are plotted in absolute J vs J-K . . . . .	14
3.1	[ $\alpha$ /Fe] measured in various parts of the galaxy from Nidever et al. (2014). The gray line represents a fiducial “high $\alpha$ ” and serves as a reference. In panels a, b, and somewhat in d, the stars can be seen to roughly follow the fiducial line. In the other panels however, especially in e, f, h, & i, there is a very obvious clump of stars in the same area in each frame, but nowhere near the fiducial line. These two separate groups of stars show the bimodal nature of the $\alpha$ -abundance distribution . . . . .	20
3.2	Taken from Bovy et al. (2012b), this figure shows the smooth $\alpha$ abundance trend they observed. Each square represents a sub-population, colored based on its scale-height. A smooth transition in color (representing a smooth transition in population scale-height) can be seen as the sub-populations transition from high- $\alpha$ to low- $\alpha$ , conflicting with the two population, bimodal $\alpha$ -abundance observations. . . . .	21
3.3	Radial [Fe/H] and [ $\alpha$ /Fe] (represented by Mg, a common $\alpha$ -abundance tracer), separated by disc thickness, as seen in Minchev et al. (2014). . . . .	22
3.4	The galactic abundance gradient reported by Yong et al. 2012 (Yong et al. 2012). Circles and squares show their data, while plus signs show the literature sample. Lines seen connecting points show the location of the same cluster measured by 2 different studies. Discrepancies of 0.2 dex or more in [Fe/H] or over 1 kpc in $R_{gc}$ can be seen between many studies . . . . .	24
4.1	The reliability of the measured color excess depends on the reliability of the assumed intrinsic color (e.g., the narrower the color distribution the better). We show here the color distributions for different stellar populations (Blue: main sequence, Red: red clump, Black: red-giant branch) derived from Padova Isochrones (Marigo et al. 2008) for different color combinations. Our method uses the $H$ -[4.5] color which has the smallest intrinsic scatter (Panel 2). . . . .	28

4.2	Sample analysis for the cluster NGC 6802 utilizing 2MASS+WISE data (Frinchaboy et al. 2010). a) Galactic latitude and longitude for all stars (gray) within the $2R_{cl}$ area to be analyzed, stars selected to be likely members from the photometry extinction analysis are shown in black. Prime APOGEE targets are circled. b) Distribution of $A_{K_s}$ for all stars in the NGC 6802 sample area, black points denote stars with $1.1R_{cl}$ within the determined mean cluster $A_{K_s}$ range. c) Color-magnitude diagram (CMD) for all stars in the analysis area (gray). The dashed box denotes the SDSS-III/APOGEE target selection region. Black points denote stars selected as likely members from their $A_{K_s}$ . d) CMD of only likely cluster members overplotted with the Padova Isochrone (Marigo et al. 2008) using the clusters parameters from Dias et al. (2002). Circled stars denote identified high-probability stars for APOGEE target selection (also see the sky distribution (a)). . . . .	32
4.3	A sample distribution of RVs in an APOGEE field (NGC 188). The cluster behavior can be clearly seen, as well as a number of field stars appropriately excluded . . . . .	34
4.4	The CMD for NGC 2420, with APOGEE member stars shown in red and non-members shown in blue, plotted over the cluster stars. An isochrone fit based on catalog parameters from Dias et al. (2002) is also shown. . .	36
5.1	The very high reliability abundance gradients using APOGEE clusters. (a) shows the entire sample, while (b) shows the sample with the very metal-rich “odd-ball” NGC 6791 removed. . . . .	39
5.2	The galactic abundance gradient within various slices of the disc, chosen so that each bin includes approximately equal numbers of clusters. $R_{GC}$ and $z$ are in kpc. . . . .	40
5.3	The galactic abundance gradient for clusters of varying age, chosen so that each bin includes approximately equal numbers of clusters. The age range is given in Gyr in the bottom right, and $R_{GC}$ is in kpc. . . . .	42

# List of Tables

3.1	A summary of reported spectroscopic abundance gradients. The number of clusters studied by the authors is given, as well as the total number of clusters used for the measurement. Quoted uncertainties are also provided (where available), and we note that the relatively low uncertainties the authors quote make many of these results incompatible. . . . .	23
5.1	A summary of reported abundance gradients broken down by age bins. Only the 3 studies mentioned in §3.3 which reported gradients broken down by age are shown. Yong et al. (2012) is omitted because no numerical gradients are for their age-binned sample. The “Young”, “Middle-Age”, and “Old” labels are given, as well as the age ranges from the studies. * A reminder that the old sample presented in this work is $> 2$ Gyr, not 4 Gyr. + We include results from current galactic chemical evolution models as well. The youngest age bin given by the authors is $a < 2$ Gyr, then $2 < a < 4$ , which we use for the middle-age bin. An average of their older age bins is given for the old bin. . . . .	44
A.1	The full sample of very high confidence clusters. The number of APOGEE stars and their mean $[\text{Fe}/\text{H}]$ are given, as well as values used for gradient analysis from Dias et al. (2002). * indicates a cluster with age $< 0.01$ Gyr, possibly estimated at as low as 1 Myr . . . . .	50

# List of Abbreviations

CMD	Color Magnitude Diagram
RV	Radial Velocity (Doppler velocity)
APOGEE	Apache Point Observatory Galactic Evolution Experiment
SDSS	Sloan Digital Sky Survey
OCCAM	Open Cluster Chemical Abundance and Mapping Survey
2MASS	2 Micron All Sky Survey
WISE	Wide-field Infrared Survey Explorer
RJCE	Rayleigh Heans Color Excess
ASPCAP	APOGEE Stellar Parameter and Chemical Abundance Pipeline
KDE	Kernel Density Estimator
HST	Hubble Space Telescope

# Chapter 1

## General Scientific Introduction

### 1.1 Astronomical Measurements

#### 1.1.1 The Magnitude System

Like much of physics, astronomy is plagued by a historical convention known as the magnitude system. Although, as with other areas of physics, it has remained because it is generally useful. The magnitude system originated with the Greek astronomer Hipparchus, who classified the brightest stars as “of the first magnitude”, down to stars “of the 6th magnitude”, which were barely visible (to the naked eye, on a clear, dark night).

Since the human eye detects brightness logarithmically, the system was consequently logarithmic, which turned out to be a good thing when it was extended, as star brightness spans several orders of magnitude. Unfortunately, it was far from rigorous. The magnitude bins were only approximate.

As astronomers gained tools to more precisely quantify brightness, it was observed that each magnitude increased in brightness by a factor of about 2.5. Since  $2.5^5 \approx 100$ , a difference in 5 magnitudes was defined to be a factor of 100 in brightness.

Using flux (energy per unit area, generally *ergs/cm<sup>2</sup>* for astronomers), the difference in flux for two objects,  $F_1$  and  $F_2$ , can be given in magnitudes,  $m_1$  and  $m_2$ , by:

$$m_2 - m_1 = 2.5 \log_{10} \left( \frac{F_2}{F_1} \right) \quad (1.1)$$

It is prudent to point out that this is merely a differential definition: there is no zero point! This means a zero point must be chosen. Older systems defined the brightness of the star Vega as the zero point, and most modern systems define a zero point very close to this. The choice is fairly unimportant, so long as the zero-point is used consistently to measure the magnitudes of different stars.

### 1.1.2 Distance

The brightness of any object, including stars, falls off as  $\frac{1}{r^2}$ . So of course, the brightness we measure is much less than the brightness near that star. We refer to the intrinsic brightness as *absolute magnitude*, and the observed brightness as *apparent magnitude*. If the absolute magnitude is known, then the difference between absolute magnitude and apparent magnitude can be used to determine the distance to an object.

Consider a source. If the flux at some distance  $D$  is  $F$ , then the flux  $f$  at some other distance  $d$  will have the relationship:

$$f = \left(\frac{D}{d}\right)^2 F, \quad (1.2)$$

which is the inverse square law for radiation. This relationship can be seen quickly by considering the case  $d = 2D$ . In such case,  $f = F/4$ . Again though, we are left with the problem of a differential system ( $d$  vs  $D$ ). To solve this problem, we define a standard distance of 10 parsec (parsecs<sup>1</sup>), at which the *absolute magnitude* is measured. If the absolute magnitude is  $M$  and the apparent magnitude is  $m$ , then given eq. 1.1 and eq. 1.2:

$$\begin{aligned} \frac{f}{F} &= \left(\frac{d}{D}\right)^{-2} \\ \log_{10} \left(\frac{f}{F}\right) &= -2 \log_{10} \left(\frac{d}{D}\right) \\ -2.5 \log_{10} \left(\frac{f}{F}\right) &= 5 \log_{10} \left(\frac{d}{D}\right) \\ m - M &= 5 \log_{10} \left(\frac{d}{D}\right) \end{aligned}$$

and using  $D = 10$  pc:

$$m - M = 5 \log(d) - 5 \quad (1.3)$$

---

<sup>1</sup>parsecs are a unit defined for measuring stellar parallax, but for this work we will simply note 1 pc  $\approx$  3.26 light years

The  $m - M$  term is often referred to as the distance modulus, for the obvious reason that distance can be deduced merely from a difference in magnitudes. This is why so much effort is given to finding absolute magnitudes in astronomy.

### 1.1.3 Photometry

When discussing brightness, in flux or magnitude, there is an ambiguity not addressed above: how much of the EM spectrum is being considered? Astronomers occasionally talk about *bolometric magnitude*, which is the flux integrated over the entire spectrum, but in practice this is less useful for most applications. It is more useful to consider only the flux in a small region of the spectrum.

Astronomers have consequently developed many “filters”, which are carefully calibrated passbands that only allow light in a certain wavelength range to pass. Figure 1.1 shows the 2MASS (§4.2.1.1) filters.

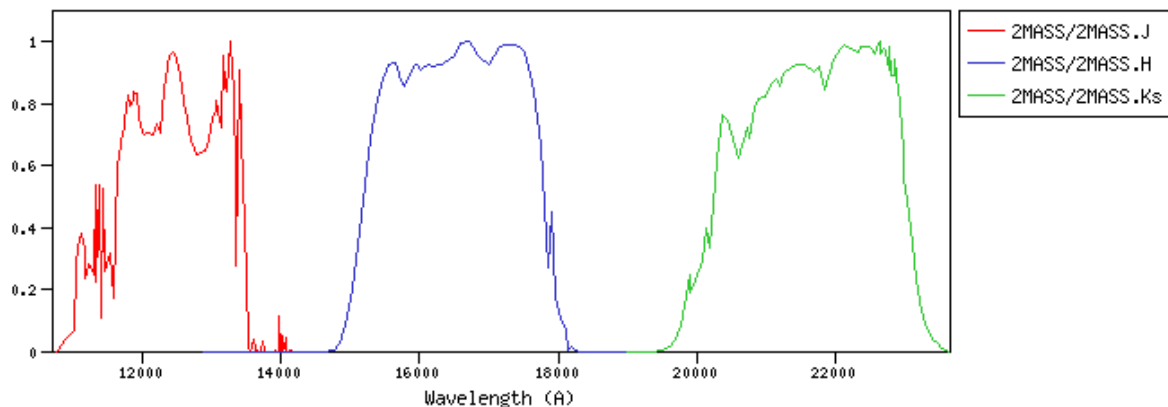


Figure 1.1: Transmission vs wavelength (in  $\text{\AA}$ ) for the 3 2MASS filters (from Rodrigo 1999)

These carefully calibrated filters allow for careful comparison between stars, and they allow astronomers to compare data from different telescopes. Using 2 different filters

also allows us to define a particularly useful measurement: color. For astronomers, the color of an object can be specified as the difference between magnitudes in 2 filters. B-V (magnitude in the “B” or blue band, minus magnitude in the “V” or visual band) is the most commonly used color, but the difference of any 2 filters defines a useful color (for example, J-K will be used commonly).

When discussing color, it is prudent to point out the mathematical oddities caused by the magnitude system running in reverse. If a star is brighter in the “B” band than in the “V” band, it will appear bluer. It will also have a *lower* “B” value than “V” value. B-V will therefore be negative. This is true in general: bluer stars have more negative colors and redder stars have more positive colors.

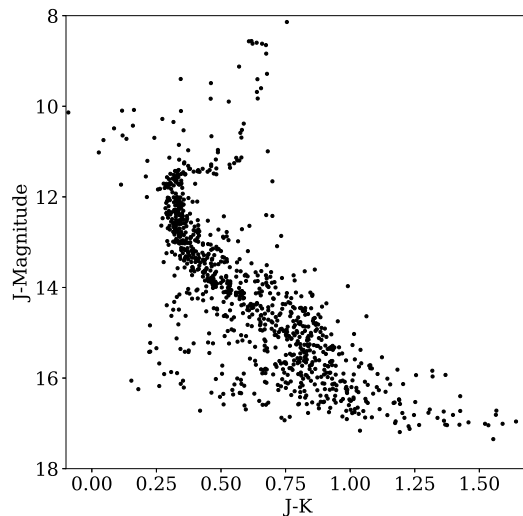


Figure 1.2: Color-Magnitude Diagram (CMD) for cluster NGC 2682

The combination of an astronomical color and brightness (“magnitude”) allows us to finally construct a Color-Magnitude Diagram (CMD). Figure 1.2 shows such a diagram for star cluster NGC 2682. The diagram is used to investigate relationships between stars,

generally stars found together on the sky (such as those in star clusters). The extended region of over-density is a pattern commonly seen in CMDs and is well understood in terms of stellar evolution, as explained below.

#### 1.1.4 Effects of Interstellar Dust

With an understanding of the photometric magnitude system and eq. 1.3, we can undertake a reasonable discussion of interstellar dust, and the problems it causes. Interstellar dust refers to particles of non-negligible size (up to nearly 1  $\mu\text{m}$ ) floating in space. Often they group into clouds, but they are present to some degree along essentially every line of sight.

Dust affects light by scattering and absorbing more blue light than red light, causing any source viewed through dust to appear not only dimmer, but redder. The more dust in front of an object, the redder it appears. This effect was first noted by Robert Trumpler (Trumpler 1930) when he was studying star clusters. He used eq. 1.3 and an approximation of intrinsic stellar parameters (gained from the spectra of some stars) to estimate the distance to these clusters. But he found a strange systematic error in the sizes of some clusters, correlated with their distance. This led him to propose the existence of some “absorbing material” along the line of sight, which we now know to be dust.

In the context of eq. 1.3, a term for the amount of light attenuated in a given passband,  $X$ , traditionally labeled  $A_X$ , can be introduced to quantify the effect of dust in magnitudes. This term has the effect of modifying eq. 1.3:

$$m - M = 5 \log(d) - 5 + A_X \quad (1.4)$$

where  $A_X$  would, appropriately, cause the source to appear dimmer in band  $X$ , as larger magnitudes correspond to fainter objects. If we consider specific bands, say B and V, we can discuss the differential effects of the dust. V is “redder” than B, so consequentially, the B band magnitude will be dimmed more by dust than the V band magnitude. This has important consequences for astronomical colors: the value of B-V will now be higher (since the magnitude system goes in reverse, B has increased by more than V due to the dust). This leads to a new term, *color excess*, labeled  $E(B-V)$ , or  $E(J-K)$ , etc, depending on which color we’re discussing, defined to be:

$$E(B - V) \equiv (B - V) - (B_0 - V_0) \quad (1.5)$$

where  $(B_0 - V_0)$  represents the intrinsic color. Realizing that  $A_B \equiv B - B_0$  and  $A_V \equiv V - V_0$ :

$$(B - V) - (B_0 - V_0) = A_B - A_V$$

$$E(B - V) = A_B - A_V$$

$E(B-V)$  is also commonly referred to as *reddening*, because the colors are literally more red.

## 1.2 Spectroscopy Basics

Spectroscopy is an essential tool for astronomers that allows us to measure flux as a function of wavelength, as opposed to photometry where flux is measured for a relatively wide range of wavelengths. In spectroscopy, flux is measured in wavelength bins of a few angstroms, for simple applications such as measuring Doppler shift, to a fraction of an angstrom, for more detailed experiments such as APOGEE (Majewski et al. 2017).

### 1.2.1 Spectral Lines and Doppler Shift

The quantum mechanical property of atoms to emit and absorb light at specific wavelengths, corresponding to electronic transitions between discrete energy levels, is now well understood. This property is very useful for astronomers when studying distance objects. For example, we find in the lab that calcium absorbs light at 8498 Å, 8542 Å, and 8662 Å; a very distinctive feature referred to as the “calcium triplet”. We may find that an object in space has a similar feature, but at 8500 Å, 8544 Å, and 8664 Å. This is of course still the calcium triplet but “redshifted” by 2 Å.

$$v = \frac{\lambda - \lambda_0}{\lambda_0} c \quad (1.6)$$

This allows us to calculate a Doppler shift (eq. 1.6) and tells us the object is moving at about 75 km s<sup>-1</sup> away from us.

## 1.2.2 Metallicity

Astronomers use the term *metallicity* to refer to the amount of “metals” in a star. But for astronomers, everything heavier than Helium is a metal! This classification is not absurd when the origin of these elements is considered. Hydrogen and helium (with some trace amounts of lithium) formed directly after the Big Bang. Everything heavier than helium was formed as the result of nuclear fusion the core of stars.

Using a variety of lines, we can start to get an idea of what an object (typically a gas cloud or a star) is made of, and thereby determine its metallicity. On the surface, it is obvious that if a star has thick carbon lines but very thin zirconium lines, there are more carbon atoms absorbing light than zirconium atoms. But the process gets much more complicated.

The process for determining actual numbers of atoms (approximately) along a line of sight requires modeling. For stars, this means modeling a stellar atmosphere. First, a model is created to determine how many absorbers are needed to produce the size (depth and width) of the line being considered. This is completed for different lines of the same element, usually representing different ionization states. By comparing the different ionization states, a temperature can be determined that would cause that distribution of ionization states. At this point, the total number of atoms for a given element, along this line of sight, can be determined.

For a star or a gas cloud, absolute numbers of atoms are enormous, and useless, because the vast majority will be Hydrogen. Astronomers are however interested in the ratio of elements relative to Hydrogen (the *metallicity*). Therefore using only the line-

of-sight measurements is sufficient (if that line of sight is representative of the object, which for stars it is; gas clouds are more problematic).

As with many astronomical quantities, metallicity tends to increase by orders of magnitude, and thus a logarithmic scale was adopted. And as with other astronomical measurement, a convenient zero point was chosen. In this case, we chose the Sun because we know the actual metal content of the Sun very well. It is convention to only use the iron (Fe) abundance to discuss the average metal content (metallicity) of the star, because in addition to being simpler, the iron abundance tends to trace the overall metal abundance very well. The final measurement is given by:

$$[Fe/H] \equiv \log_{10} \left( \frac{N_{Fe}}{N_H} \right)_{\star} - \log_{10} \left( \frac{N_{Fe}}{N_H} \right)_{\odot} \quad (1.7)$$

So a metallicity  $[Fe/H] = 0$  means “equal to solar abundance”, while  $[Fe/H] = 1$  means “10 times greater than solar abundance”, and  $[Fe/H] = -1$  means “10 times less than solar abundance”.

### 1.3 Star Clusters

Star clusters are powerful tools for astronomers. Star clusters are the birth place for nearly all stars, usually consisting of thousands to nearly a hundred thousand stars. They form out of a giant molecular cloud (GMC), consisting of primarily hydrogen gas with some helium and generally less than 1% “metals” (elements heavier than helium), these clouds contain millions of solar masses ( $M_{\odot}$ ) of material, and can be over 100 parsecs in size. Gravity causes the cloud to collapse collapse into stars (see §1.4).

Since all stars in a star cluster formed from the same material, they maintain similar chemical signatures. Perhaps most importantly, all stars in the cluster are the same age (give or take a few million years, which is within the realm of error on an astronomical time line).

The uniform nature of the chemical composition and ages of stars in open clusters allows them to be modeled with relative ease (see §1.5) which allows a distance and age to be determined fairly accurately. This means there are star clusters scattered around the Galaxy with (relatively) easily obtainable ages, distances, and chemical composition, leading to their use as tracers of chemical abundance within the galaxy.

## 1.4 Stellar Evolution

After many years of developing models of stellar formation, interiors, and atmospheres, and comparing to observations, astronomers have a decent understanding of the life cycle of stars. As discussed above, stars form from a GMC through gravitational collapse. The gravitational collapse causes much of the gravitational potential energy to be converted into thermal energy, causing particles to resist further collapse. The current understanding of the mechanism to overcome this runaway thermal problem involves heavier elements and molecules inside the cloud. They are able to absorb some of the thermal energy and radiate it away from the cloud more readily than hydrogen. This mechanism remains important after the star has formed, because ionized hydrogen is inefficient at radiating energy. This is why the initial chemical composition of the cloud has an impact on stellar evolution (we will return to this idea when discussing isochrones §1.5).

If enough mass from the cloud collapses together, eventually the pressure and temperature at the center of the collapse will be great enough to ignite hydrogen fusion. Hydrogen fusion begins releasing energy and prevents further collapse. The star is now on the “main sequence”, where it spends the majority of its life.

For lower mass stars, eventually a significant amount of helium ash will build up in the core, which the star is not hot or dense enough to fuse yet. When the star is out of hydrogen to burn in its core it begins to contract gravitationally, causing the temperature around the shell (and in the core) to increase even more, leading to an increase in hydrogen fusion in the shell. The contraction has the reverse effect on the outer layers, causing them to become less dense and cool, thus increasing their opacity (i.e. the amount of photons they absorb). The increased opacity leads directly to the expansion of these outer layers into red giants, as more photon flux from fusion in the hydrogen shell is “caught” by these more opaque layers.

As the star runs low on hydrogen in the remaining envelope of fusion, outward radiative pressure from fusion decreases and gravitational pressure increases until it is sufficient to ignite helium fusion. At this point, massive quantities of helium ignite almost simultaneously in a phenomenon known as the “helium flash”. The remaining helium burns slowly in what is often referred to as the “helium main sequence”. This helium main sequence is short lived, and similarly to hydrogen, soon only a shell of burning helium remains. Eventually, only the hot, inert core remains (mostly carbon and oxygen from helium fusion), under enough pressure to become electron degenerate, but not to break that degeneracy. This remnant is known as a white dwarf.

More massive stars are able to continue fusing progressively heavier elements in their cores after the “helium main sequence”, until they’re fusing iron into nickel. Since  $\text{Fe} \rightarrow \text{Ni}$  fusion requires more energy than it releases, the core stops releasing energy, destroying the hydrostatic equilibrium and leading to a core collapse. The result is a large explosion, potentially a supernova, leaving behind a neutron star or, if enough mass remains to overcome the neutron degeneracy pressure, a black hole.

## 1.5 Isochrones

Based on our knowledge of stellar evolution, it is possible to know the brightness, mass, size, and temperature of a star of a given mass and initial chemical composition, at any time since it formed. We can make these predictions for a collection of stars of a variety of initial masses in order to model the behavior of a group of stars over time.

The power of predicting the group behavior mostly revolves around star clusters. As noted earlier, the over densities seen in Figure 1.2 are seen in the CMDs of all star clusters. These patterns arise because stars constitute a single stellar population, and they can be reproduced by models. These models are known as *isochrones* (from the Greek, *isos*: equal, & *chronos*: time), and appropriately: they show a population of stars all the same age. The models are generated by evolving a number of stars of different initial masses, but the same initial chemistry, through a range of time steps, generally starting around 60 million years, when the most massive stars have destroyed themselves and only the well behaved remain, and continuing to an age of around 10 billion years, when most average stars have at least begun to evolve into giants. The left panel of

Figure 1.3 shows the evolution of an isochrone over a few billion years, and the right panel shows the effect initial chemistry can have on the evolution of a star cluster after 1 Gyr.

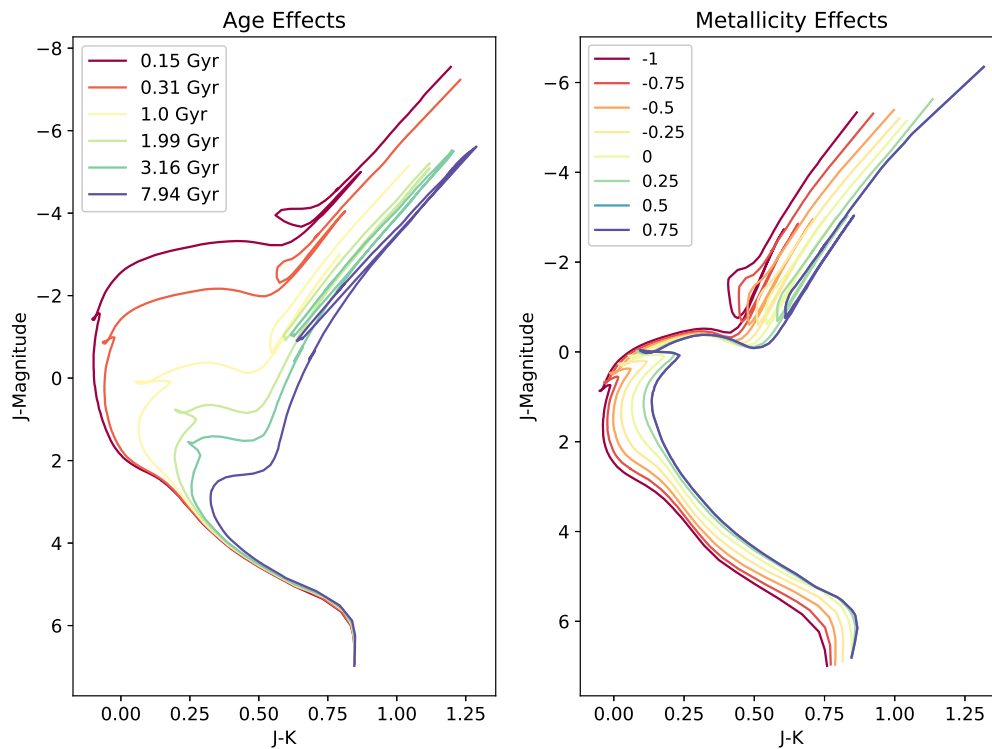


Figure 1.3: Left: The evolution of an isochrone of constant metallicity over a range of ages in Gyr, Right: a sample of 1 Gyr isochrones spanning a range of metallicities  $[\text{Fe}/\text{H}]$  (see below). Both are plotted in absolute J vs J-K

### 1.5.1 Isochrone Fitting

Since isochrones model star clusters so well, it is very common to fit isochrones to cluster CMDs. This can be done a number of ways, with varying degrees of success due the difficulty of reliably constraining the fit. Figure 1.3 shows just how much the isochrone can shift (i.e. become redder and dimmer) as it grows older, or more metal-rich, leading to a

number of well known degeneracies between isochrones of different ages and metallicities. With no prior knowledge of the cluster, large uncertainties in age and metallicity from an isochrone fit are unavoidable.

Fitting the isochrone involves a 4 dimensional parameter space; besides age and metallicity,  $m-M$  and  $E(B-V)$  must be determined as well.  $m-M$  is determined by shifting the entire isochrone in magnitude space, moving from intrinsic brightness ( $M$ ) to observed brightness ( $m$ ), and is directly related to the distance to the cluster (see §1.1.2).  $E(B-V)$  (line-of-sight reddening, see §1.1.4) can be seen as shifting the entire isochrone in  $(B-V)$  (or  $J-K$ , or any color). However, recent work (Correnti et al. 2016) has reinforced the need to apply a reddening correction to the synthetic spectra from the isochrone models before convolving filter functions to estimate absolute magnitudes, and not simply shift along the color-axis.

A good isochrone fit then can establish both the age and distance to a cluster, within some margin of error, as well a somewhat crude metallicity measurement (not nearly as accurate or precise as a spectroscopic measurement). All of the values used in this work come from fitting done by Dias et al. (2002), or fitting they compiled from the literature.

# Chapter 2

## Objectives

**What are the abundance gradients in the Galactic disc, and how do they vary as a function of the age and location of the tracer population?**

The most recent National Academy Decadal Survey of Astronomy & Astrophysics (Council et al. 2011) identified key challenges in astrophysics: interpreting the “fossil record” of galaxy assembly; mapping the flows of mass, energy, and chemical elements within galaxies; and characterizing the relationship between ordinary matter and the mysterious “dark matter.” We will map the fossil record in the chemistry of the Milky Way disc using the most reliable age-datable tracer, *open star clusters*.

Open clusters provide the only reliable ‘multi-age’ population tracer in the Galactic disc with which the *radial metallicity gradient* of the disc can be measured; one of the basic chemical measurements of the Milky Way disc. This measurement has been made many times with most gradients being measured to be between  $-0.05 \text{ dex kpc}^{-1}$  (Reddy et al. 2016) and  $-0.09 \text{ dex kpc}^{-1}$  (Yong et al. 2012, Friel 1995, Carraro et al. 1998). One of the key factors in the spread of gradients has been the use of literature compiled

samples from studies using different telescopes and different instruments, with only 1–2 stars measured per cluster and 2–5 clusters measured per study, yielding large systematic offsets in the compiled sample.

The problem is stated well by Yong et al. (2012):

*... that definitive conclusions await homogeneous analyses of larger samples of stars in larger numbers of clusters. Arguably, our understanding of the evolution of the outer disc from open clusters is currently limited by systematic abundance differences between various studies.*

We have created the largest catalog of open clusters with chemical parameters determined using a *uniform* instrument, telescope, and pipeline, and we use this catalog to make the first *uniform* measurement of the galactic radial metallicity gradient based on more than a few clusters. Since our sample is large enough to meaningfully distinguish populations of different ages, and open clusters are reliable age tracers, we also investigate trends in this gradient as a function of the age of the population.

# Chapter 3

## Chemical Evolution of the Galactic Disk

### 3.1 Galactic Structure

While the Milky Way provides the most detailed laboratory for studying a galaxy, being within the Galaxy imposes harsh constraints on the overall structure we are able to observe. For this reason, much of our understanding of galaxy evolution is based on observations of other galaxies.

Astronomers have studied the brightness profiles and stellar density distributions of other galaxies for decades and generally find exponential trends of some form (de Vaucouleurs 1959). The most accurate description of the profile perpendicular to the disc of nearby galaxies and the Milky Way is found to be a two-component model, referred as the “thick” and “thin” discs (Burstein 1979, Gilmore & Reid 1983). While estimates

of the photometric scale-lengths<sup>1</sup> of these discs are relatively well constrained for other galaxies, estimates for the Milky Way vary greatly and are not necessarily in agreement with those of galaxies assumed to be similar to the Milky Way (Bland-Hawthorn & Gerhard 2016).

Studies have shown (e.g. Bensby et al. 2005) the thin disc to be characterized by kinematically “cooler” stellar populations with near solar  $\alpha$ -abundance<sup>2</sup> while the thick disc is observed to be enriched in  $\alpha$ , kinematically “hotter”, and generally older. This bimodality in  $\alpha$  is well documented (Nidever et al. 2014, Bensby et al. 2005), and can be seen clearly in Figure 3.1. However, some studies suggest that there is no meaningful distinction between the “thick” and “thin” discs (Bovy et al. 2012a). Rather, a distribution of sub-populations with a smooth change in chemical abundances may better describe observations. This trend can be clearly seen in Figure 3.2.

## 3.2 Galactic Chemical Evolution Models

Models of a smoothly varying disc also show that the largest scale-height sub-component is located near the center of the galaxy, suggesting that the trends we see are the results of internal galactic evolution (Bovy et al. 2012b). On the other hand, in order to explain a bimodal trend, more complicated models requiring complex gas inflows and outflows as well as radial mixing are required (Andrews et al. 2017). But not all of these more complicated models predict a bimodal trend. The model of Minchev et al. (2013) predicts

---

<sup>1</sup>scalelength: the distance required for a quantity, such as brightness or density, to decrease by a factor of  $1/e$

<sup>2</sup> $\alpha$  elements are those built up by fusing He nuclei ( $\alpha$  particles)

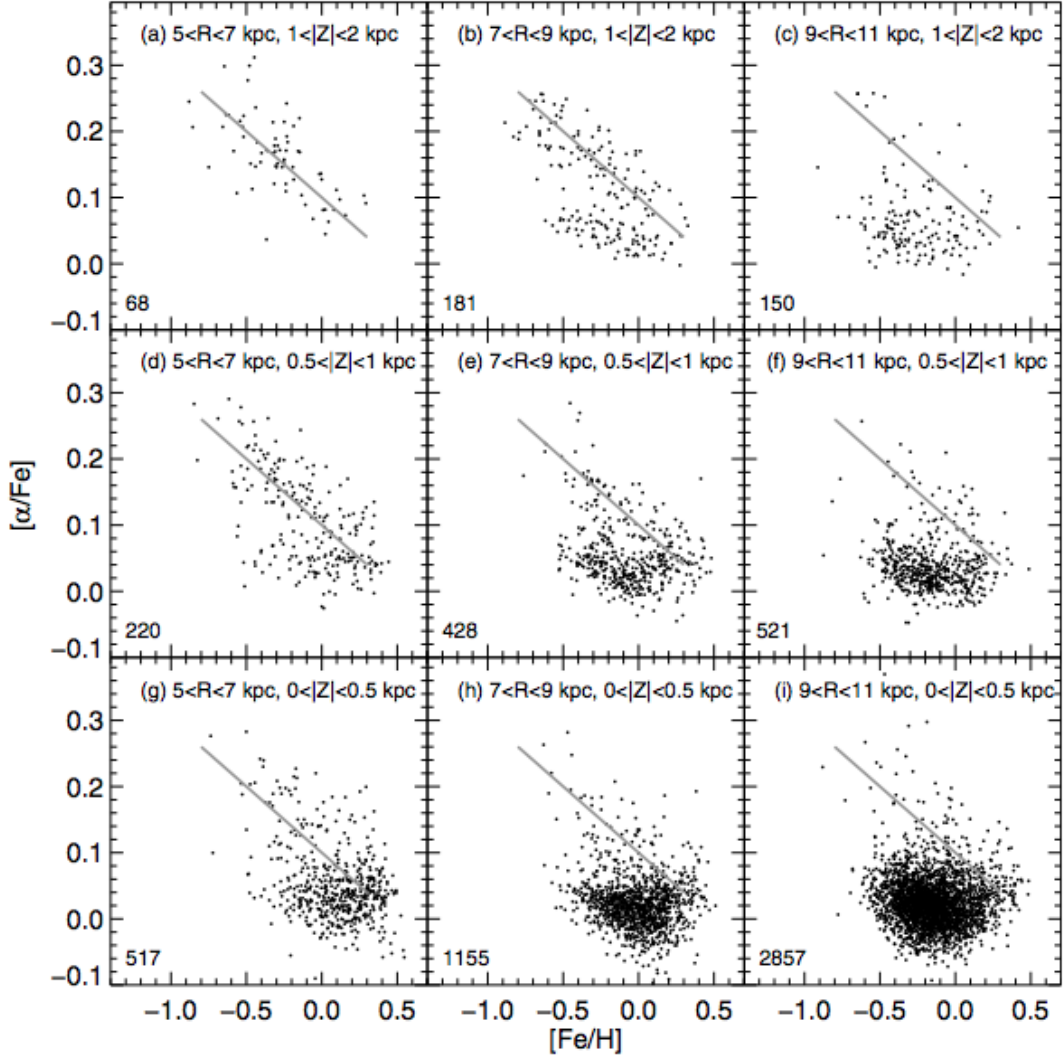


Figure 3.1:  $[\alpha/\text{Fe}]$  measured in various parts of the galaxy from Nidever et al. (2014). The gray line represents a fiducial “high  $\alpha$ ” and serves as a reference. In panels a, b, and somewhat in d, the stars can be seen to roughly follow the fiducial line. In the other panels however, especially in e, f, h, & i, there is a very obvious clump of stars in the same area in each frame, but nowhere near the fiducial line. These two separate groups of stars show the bimodal nature of the  $\alpha$ -abundance distribution

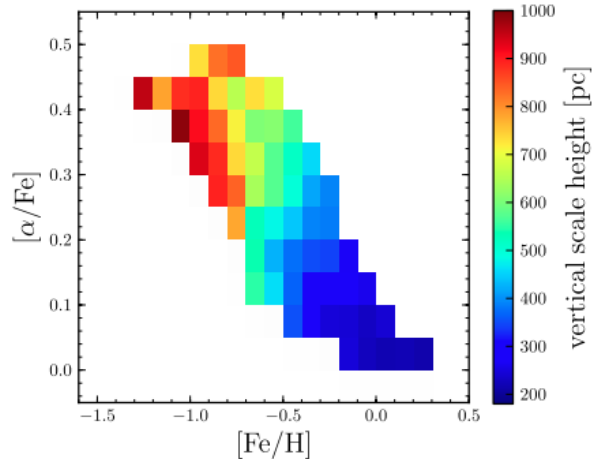


Figure 3.2: Taken from Bovy et al. (2012b), this figure shows the smooth  $\alpha$  abundance trend they observed. Each square represents a sub-population, colored based on its scale-height. A smooth transition in color (representing a smooth transition in population scale-height) can be seen as the sub-populations transition from high- $\alpha$  to low- $\alpha$ , conflicting with the two population, bimodal  $\alpha$ -abundance observations.

very similar results to those observed by Bovy et al. (2012b) (Figure 3.2), and further suggests that the bimodal trend in  $\alpha$  can be the result of selection effects, depending on the survey, although they admit in later work its appearance in so many surveys indicates it may be a real feature (Minchev et al. 2014).

In a sense, these discrepancies are good: the different models predict different observable phenomena, thus one can be chosen. Unfortunately, adequate observations have proven difficult. But  $[\alpha/\text{Fe}]$  is far from the only observable being studied. Minchev et al. (2014) report on a variety of chemical trends which can be seen radially in the disc and in populations of different ages. Radial trends, age trends, and combinations thereof are easily obtained from galactic evolution models, and thus provide key observational constraints. Figure 3.3 shows the detailed nature of prediction obtained by modelers; we note the consistent negative gradient and flattening out towards the edge of the disc. Similar predictions can be found in Kubryk et al. (2015).

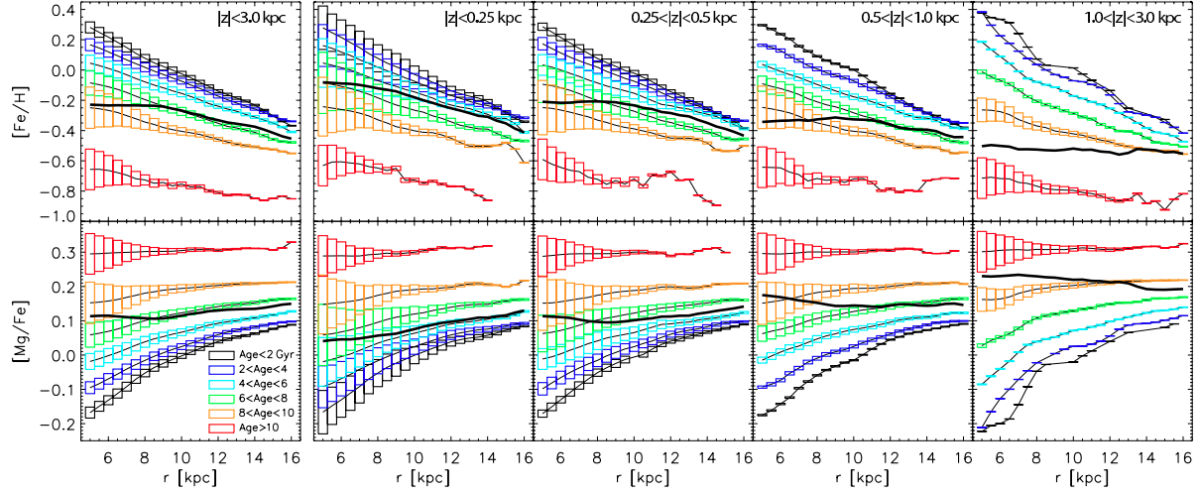


Figure 3.3: Radial  $[\text{Fe}/\text{H}]$  and  $[\alpha/\text{Fe}]$  (represented by Mg, a common  $\alpha$ -abundance tracer), separated by disc thickness, as seen in Minchev et al. (2014).

### 3.3 Recent Work

Due to their importance in constraining galactic evolution, chemical abundance gradients are commonly studied observationally. The spatial nature of the measurement requires that a reliable distance to the observed object be determined, and this severely limits candidates for observation. Variable stars called Cepheids are sometimes used, because their variability directly relates to their intrinsic brightness. However, open clusters are even more useful, because not only can their distance be determined, but their ages can be determined fairly reliably as well (see §1.3). Recent work using open clusters has consistently found a negative gradient between roughly  $-0.05 \text{ dex kpc}^{-1}$  (Reddy et al. 2016) and  $-0.09 \text{ dex kpc}^{-1}$  (Yong et al. 2012, Friel 1995, Carraro et al. 1998). Others have reported qualitatively similar gradients, but do not quote a gradient due to lack of numbers or some other limiting factor (Donati et al. 2015, Magrini et al. 2015). A summary of gradients reported by major studies in the literature can be found in Table 3.1. Studies which studied only very old or very young clusters are excluded, as are those

Study	dex kpc <sup>-1</sup>	$\pm$	# study	# total
Friel & Janes (1993)	-0.09	0.02	24	33
Friel (1995)	-0.091	0.014	0	44
Carraro et al. (1998)	-0.09	N/A	0	37
Friel et al. (2002)	-0.06	0.01	24	39
Pancino et al. (2010)	-0.06	0.02	5	57
Jacobson et al. (2011)	-0.085	0.019	10	19
Yong et al. (2012)	-0.09	0.01	5	49
Reddy et al. (2016)	-0.052	0.011	28	79

Table 3.1: A summary of reported spectroscopic abundance gradients. The number of clusters studied by the authors is given, as well as the total number of clusters used for the measurement. Quoted uncertainties are also provided (where available), and we note that the relatively low uncertainties the authors quote make many of these results incompatible.

which only quoted a gradient for a portion of the disc not studied in this work.

There is one problem immediately obvious from Table 3.1: the incompatibility of the measured gradients. Of course this may be due to under-quoted uncertainties (indeed, the quoted uncertainties seem quite small, especially when considering the quality of the fits, e.g. Figure 3.4). There may be an even better explanation for this discrepancy though, and it can be seen in the fourth column. With the exception of Friel et al. 2002, all of these studies collected the majority of the clusters used in their measurement from the literature (and the sample from Friel et al. (2002) was still almost 40% literature compiled). Both the distance and chemical abundance measurements for a cluster involve modeling and making choices, so systematic differences between studies are unavoidable. The problem can be seen clearly in Figure 3.4, taken from Yong et al. (2012): the lines connecting some points show the discrepancies between studies. If we suppose the discrepancies in the figure are representative, then the entire gradient could easily double, or be cut in half by moving those points within that error.

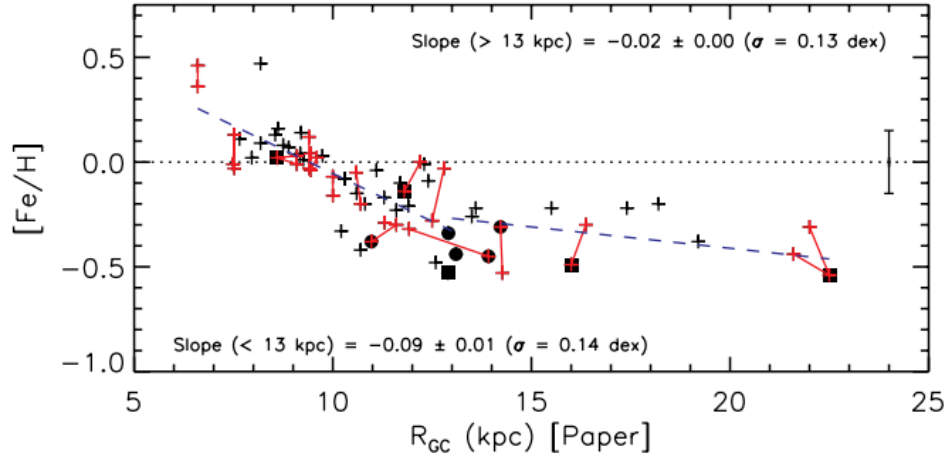


Figure 3.4: The galactic abundance gradient reported by Yong et al. 2012 (Yong et al. 2012). Circles and squares show their data, while plus signs show the literature sample. Lines seen connecting points show the location of the same cluster measured by 2 different studies. Discrepancies of 0.2 dex or more in  $[\text{Fe}/\text{H}]$  or over 1 kpc in  $R_{gc}$  can be seen between many studies

The need for an open cluster sample that can eliminate the systematic offsets between the measurements of different groups is clear. Netopil et al. (2016) present a sample of over 172 open clusters, however the metallicities presented are determined using well calibrated photometric filters. They present a handful of gradient measurements, notably: a gradient within  $R_{gc} < 12\text{kpc}$  of  $-0.066 \pm 0.007$ . While the results are significant, and fulfill the desire for a uniform system, the photometric metallicities are much less reliable than spectroscopy.

### 3.3.1 Variation with Location and Age

As stated, these gradients provide a key observational constraint to chemical evolution models of the Milky Way. The simple measurement of “a gradient” is not the most useful constraint though. Figure 3.3 from the models of Minchev et al. (2014) shows gradients in four bins in Z-height (and an “overall” gradient), and for five different stellar age bins

(and an “all the ages” bin). Since open clusters are age tracers, they can be used to test age-dependent predictions. The largest sample in Table 3.1 is 79 clusters. Supposing they were somehow able to evenly fill those twenty bins, barely four would be included in each bin. However, looking at only age bins or only  $Z$ -height bins is now possible for samples of  $> 10$  clusters.

Yong et al. (2012) investigate three age bins (age $<2$  Gyr, 2 Gyr $<$ age $<5$  Gyr, & age $>5$ Gyr), and find that the spread (away from the best fit line for the whole sample) increases with age. Jacobson et al. (2011) use different bins (age $<0.8$  Gyr, 0.8 Gyr $<$ age $<4$  Gyr, & age $>4$ Gyr). Their data may show a similar spread as age increases, but importantly, they note a change in gradient from their middle-age sample (quoted in Table 3.1), which may be as shallow as  $-0.083$  dex  $\text{kpc}^{-1}$ , (depending on two problematic clusters) to their old sample, which may be as steep as  $-0.134$  dex  $\text{kpc}^{-1}$  (depending on a problematic cluster for which one of two values for  $[\text{Fe}/\text{H}]$  could be adopted). They don’t quote a gradient for their young sample, due to it being only four clusters. Friel & Janes (1993) used the same age bins, and found a similar trend (increasing gradient with age), with gradients of  $-0.023$ ,  $-0.053$ , &  $-0.075$ ; all shallower than Jacobson et al, but the agreement in trend is certainly important. Carraro et al. (1998) also use the same age bins, and find a similar trend with gradients of  $-0.06$ ,  $-0.11$ , &  $-0.12$ . However, they subdivide the oldest bin and investigate an age $>6$  Gyr sample as well, which they find to have a gradient of  $-0.08$ , somewhat confounding the trend.

### 3.3.2 The Open Cluster Chemical Abundance and Mapping (OCCAM) Survey

The need for an open cluster sample that can eliminate the systematic offsets between the measurements of different groups is clear. The Open Cluster Chemical Abundance and Mapping (OCCAM) survey provides the answer to this problem. The OCCAM survey will use a *uniform* set of chemical measurements, made using the same instrument and the same reduction pipeline, to investigate a large sample of open clusters.

# Chapter 4

## The Open Cluster Chemical Abundance & Mapping Survey

A number of sources underpin the OCCAM survey. Different projects are more successful at measuring different quantities, thus we have leveraged strengths from three different large surveys.

### 4.1 The APOGEE Survey

The primary analysis data for OCCAM comes from the Apache Point Observatory Galactic Evolution Experiment (APOGEE; Majewski et al. 2017) that is part of the Sloan Digital Sky Survey-III and IV surveys (SDSS; Eisenstein et al. 2011, Blanton et al. 2017), utilizing the 2.5 m Sloan Foundation telescope (Gunn et al. 2006) at Apache Point Observatory. APOGEE is a mid-infrared (1.514  $\mu\text{m}$  to 1.696  $\mu\text{m}$ ) spectroscopic survey, primarily focusing on the galactic disk. The survey uses fibers to capture the light from

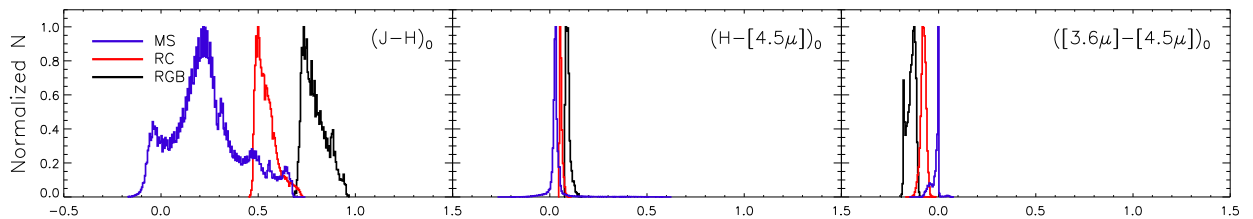


Figure 4.1: The reliability of the measured color excess depends on the reliability of the assumed intrinsic color (e.g., the narrower the color distribution the better). We show here the color distributions for different stellar populations (Blue: main sequence, Red: red clump, Black: red-giant branch) derived from Padova Isochrones (Marigo et al. 2008) for different color combinations. Our method uses the  $H-[4.5]$  color which has the smallest intrinsic scatter (Panel 2).

a single star and send it to a spectrograph, allowing for simultaneous observation of 300 stars. In this manner, the APOGEE survey has observed over 200,000 stars to date.

The APOGEE data reduction pipeline (García Pérez et al. 2016) uses the spectra to determine radial velocities (RV), from the Doppler shift, as well as a number of intrinsic parameters for each star, obtained by modeling the stellar atmosphere, including a number of elemental abundances. APOGEE provides high precision radial velocities (RVs), stellar parameters ( $T_{eff}$ ,  $\log g$ ,  $[M/H]$ ,  $[C/M]$ ,  $[N/M]$ ,  $[\alpha/M]$ ), and eventually detailed abundances for individual elements (Fe, C, N, O, Al, Si, Ca, Ni, Na, S, Ti, Mn, K, Cu, and possibly more). The APOGEE data provide the *uniform* chemical data that underpin this study.

## 4.2 Identifying Member Stars in OCCAM Open Clusters

### 4.2.1 Likely Member Targeting

The OCCAM survey utilized two primary photometry datasets in selecting targets:

#### 4.2.1.1 Photometry

In order to select targets for APOGEE observations, 2 uniform, all-sky photometry datasets were used: 2MASS and WISE. 2MASS photometry is also used to create infrared CMDs highlighting APOGEE stars.

The 2 Micron All Sky Survey (2MASS Cutri et al. 2003) was one of the earliest and most digital ambitious all-sky surveys. Running from 1997 to 2001, the survey required two telescopes in separate hemispheres to complete the project. The data (released to the public) included 300 million observed objects, primarily stars. The data consist of photometric measurements in the near infrared bands J, H, &  $K_s$ , down to a magnitude of around 16 in the H band.

The Wide-field Infrared Survey Explorer (WISE; Wright et al. (2010)) is a NASA infrared space based telescope that surveyed the entire sky in the mid-infrared (photometric bands centered at 3.4  $\mu\text{m}$ , 4.6  $\mu\text{m}$ , 12  $\mu\text{m}$ , & 22  $\mu\text{m}$ ).

#### 4.2.1.2 OCCAM target selection

The combination of 2MASS and *WISE* photometry allows a direct assessment of the line-of-sight reddening to any particular star. The long wavelength regime of spectral energy distributions (SEDs) of stars have the same Rayleigh-Jeans shape, equivalent to saying that the Vega-based, *intrinsic* colors of all stars are nearly constant for the correct combination of filters (Figure 4.1). Thus, the *observed* mid-IR colors contain information on the reddening to a star *explicitly*, whereas the NIR SEDs contain information on the stellar types. By assuming constancy of the intrinsic stellar ( $H-4.5\mu\text{m}$ ) colors in the Rayleigh-Jeans regime,  $E(H-4.5\mu\text{m})$  is derived directly from the observed ( $H-4.5\mu\text{m}$ ) color. The spread from different populations, RGB, red clump and main sequence, is minimized for this combination yielding an intrinsic spread of less than 0.09 mag in color for all but the reddest and bluest stars. Since the primary purpose in using this technique is to “clean” the cluster from the field, small systematics are not a concern. Also, the reddest main sequence stars that would belong to a cluster are too faint for these surveys.

Frinchaboy et al. (2010) have devised a technique to utilize the extinction ( $A_{K_S}$ ) derived from the Rayleigh Jeans Color Excess (RJCE) technique (Majewski et al. 2011 and described above), to distinguish and isolate star cluster stars from foreground and background contamination. This technique consists of isolating a region of approximately twice the cluster’s catalog radius (Dias et al. 2002) and dividing it into 5 regions (see Figure 4.2a). We utilize four “background” regions and the cluster region (radius =  $R_{Dias}$ ). The background is divided in order to account for dust clouds and any other source of background variability.

We subtract the mean field/background star numbers from the “cluster” star numbers within a given  $A_{K_s}$  range, and scan this range across all available  $A_{K_s}$  values that have at least 15 stars (see Figure 4.2b). The window of extinction with the highest concentration of stars within the inner radius will reveal the cluster (Figure 4.2c & d). We then work to optimize the cluster isolation surveying a grid of  $A_{K_s}$  width,  $A_{K_s}$  stepsize, and allowed  $\sigma_{A_{K_s}}$  values.

We present a demonstration of the technique utilizing the cluster NGC 6802, shown in Figure 4.2. Figure 4.2a first shows the area explored by our analysis in Galactic latitude and longitude. As described above, we selected likely cluster members utilizing the  $A_{K_s}$  as shown in Figure 4.2b. For NGC 6802 we find a low, but non-negligible extinction or reddening to the cluster. A CMD of the clusters (Figure 4.2c) is generated which highlights the member stars with  $A_{K_s}$  values within the selected window of extinction, where the dashed box denotes the area where the SDSS/APOGEE project selects targets ( $8.0 < H < 12.2$  and  $J - K_S \geq 0.5$ ). Finally, we compare our “cleaned” cluster CMD to the Padova isochrone (Marigo et al. 2008) utilizing catalog values Dias et al. (2002) for NGC 6802 and find a good match. By comparing the CMD with isochrone values, when available, we are able to isolate candidate open cluster stars with a high probability for membership.

#### 4.2.2 OCCAM Spectroscopic Observed Stars - SDSS DR14

Targets selected for analysis were observed from August 2011 to July 2014 (APOGEE-1), and from July 2014 to July 2016 (APOGEE-2). These data were released as part of the

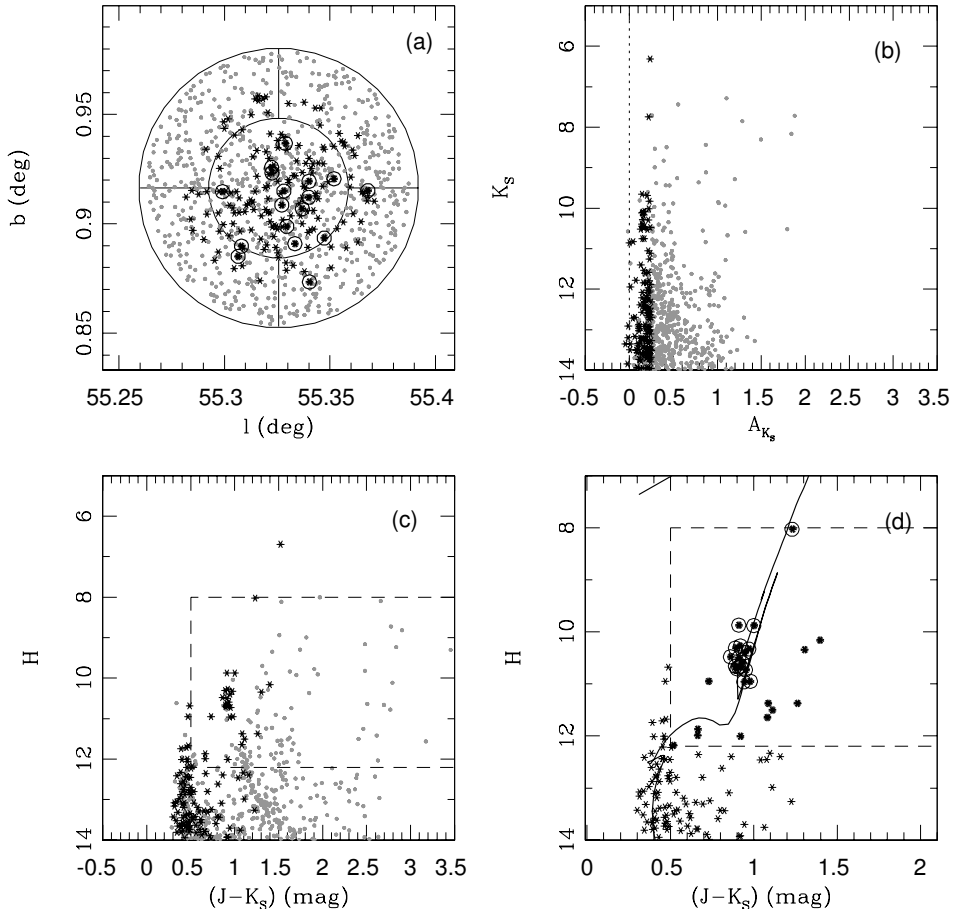


Figure 4.2: Sample analysis for the cluster NGC 6802 utilizing 2MASS+WISE data (Frinchaboy et al. 2010). a) Galactic latitude and longitude for all stars (gray) within the  $2R_{cl}$  area to be analyzed, stars selected to be likely members from the photometry extinction analysis are shown in black. Prime APOGEE targets are circled. b) Distribution of  $A_{K_s}$  for all stars in the NGC 6802 sample area, black points denote stars with  $1.1R_{cl}$  within the determined mean cluster  $A_{K_s}$  range. c) Color-magnitude diagram (CMD) for all stars in the analysis area (gray). The dashed box denotes the SDSS-III/APOGEE target selection region. Black points denote stars selected as likely members from their  $A_{K_s}$ . d) CMD of only likely cluster members overplotted with the Padova Isochrone (Marigo et al. 2008) using the clusters parameters from Dias et al. (2002). Circled stars denote identified high-probability stars for APOGEE target selection (also see the sky distribution (a)).

14th Data Release of the Sloan Digital Sky Survey (DR14; Abolfathi et al. 2017). All APOGEE data, from the beginning of APOGEE-1, were reduced using the latest data reduction pipeline. In this study, we have analyzed 2627 stars within  $2\times$  the cluster radius (Dias et al. 2002) for 49 clusters that resulted in at least 5 member stars identified

as described below (§4.2.3). Uncalibrated ASPCAP abundances from the data pipeline were used to determine membership, however only calibrated ASPCAP parameters were used to determine the reported cluster  $[\text{Fe}/\text{H}]$ . The resulting member stars cover a wide range in temperature ( $T_{eff}$ ) of 3597–7809 K, and a range in surface gravity ( $\log(g)$ ) of 0.78–3.63 dex.

### 4.2.3 OCCAM Observed Membership Criteria

Besides having similar (nearly identical) chemical properties, every star in a cluster is also gravitationally bound. Hence, they must all have similar velocities, allowing for some internal dispersion due to stars orbiting the cluster’s center of mass. Fortunately the APOGEE survey provides a velocity measurement along our line of site, RV. When compared then, 2 or more stars thought to be in the same cluster should have similar RVs, within some error accounting for the internal motion of the cluster.

Using Fe/H for the initial chemical discriminator (assuming otherwise solar abundance ratios), and RV, APOGEE data alone can provide a first guess at membership by obtaining the “bulk” RV and Fe/H for the cluster region on the sky and comparing each star to this average.

#### 4.2.3.1 Quantizing Membership Probability

The bulk behavior is found by convolving all measurements using a Gaussian kernel smoothing routine. Each star is assumed to be the center of a Gaussian, and the resultant Gaussians are effectively added together, as in Figure 4.3. In order to distinguish the cluster from field stars, 2 samples are computed: stars within 2 cluster radii of the

cluster center, and stars between 1 and 2 cluster radii of the center (technically outside the cluster). The results from the “outer” stars are subtracted from the “total” result, ideally leaving only the cluster.

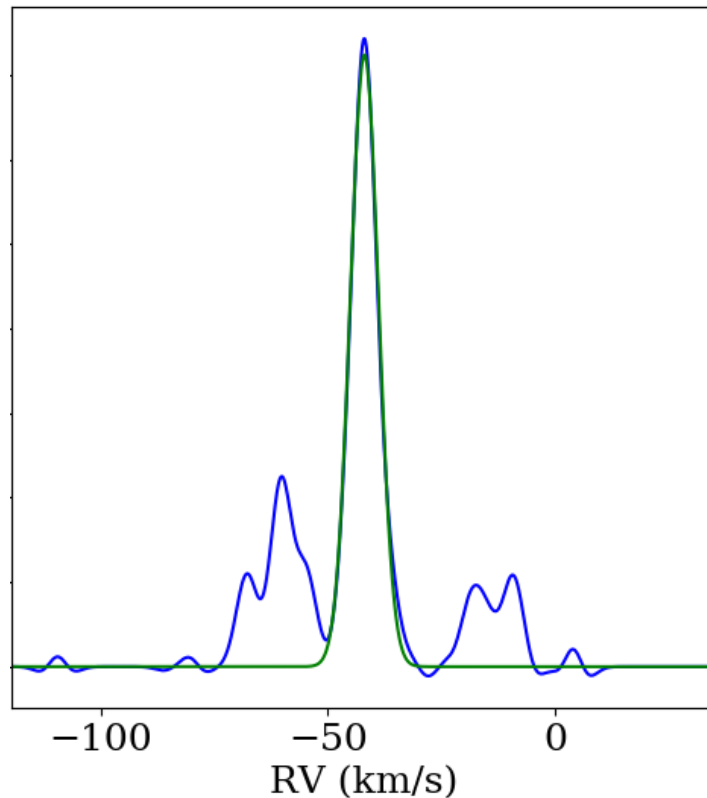


Figure 4.3: A sample distribution of RVs in an APOGEE field (NGC 188). The cluster behavior can be clearly seen, as well as a number of field stars appropriately excluded

This process is carried out for RV and Fe/H<sup>1</sup>. If there were at least 2 APOGEE stars that were cluster members, the smoothing routine will leave behind a large peak where their values combined. The shape is approximately Gaussian, so a Gaussian profile is fit. When normalized, this peak can be used as a probability distribution in RV or Fe/H space. An RV and Fe/H membership probability can then be generated for each star.

<sup>1</sup>here, we use the raw, uncalibrated [Fe/H], reported in the ‘FPARAM’ array in DR14, because calibrated abundance parameters aren’t reported for stars that fail certain checks, and the uncalibrated values are at least internally consistent, which is all this method requires

In practice  $\sigma$  tends to be fairly small, thus a  $2\sigma$  criterion is adopted for likely membership: a star with parameters falling in a  $2\sigma$  range in **both** Fe/H and RV is considered a likely member of the cluster.

The relatively low computational cost of testing every combination of over-densities in Fe/H and RV space encouraged the development of an automated routine. The combination that results in the most likely members, according to the above criteria, is adopted as the value, and membership probabilities for every star in the field are assigned accordingly.

#### 4.2.3.2 Verifying Membership

Since clusters represent a single stellar population, all stars in the cluster should fit to a single isochrone model. An isochrone fit then can provide a check on the established membership criteria. Figure 4.4 shows an isochrone fit to the open cluster NGC 2420 based on Dias et al. (2002), with APOGEE members shown in red and non-members in blue. The isochrone fit is certainly not perfect (this will be significantly improved in future work, see §6.1), however the general behavior of the cluster can be seen. The members are near to the isochrone, and very plausibly in the cluster. While some members may have been falsely rejected, obvious non-members are clearly rejected. While it certainly is possible to devise a better metric for verifying the membership (and in the future, one will be developed), the CMD comparison presented shows that the method is at least fairly reliable.

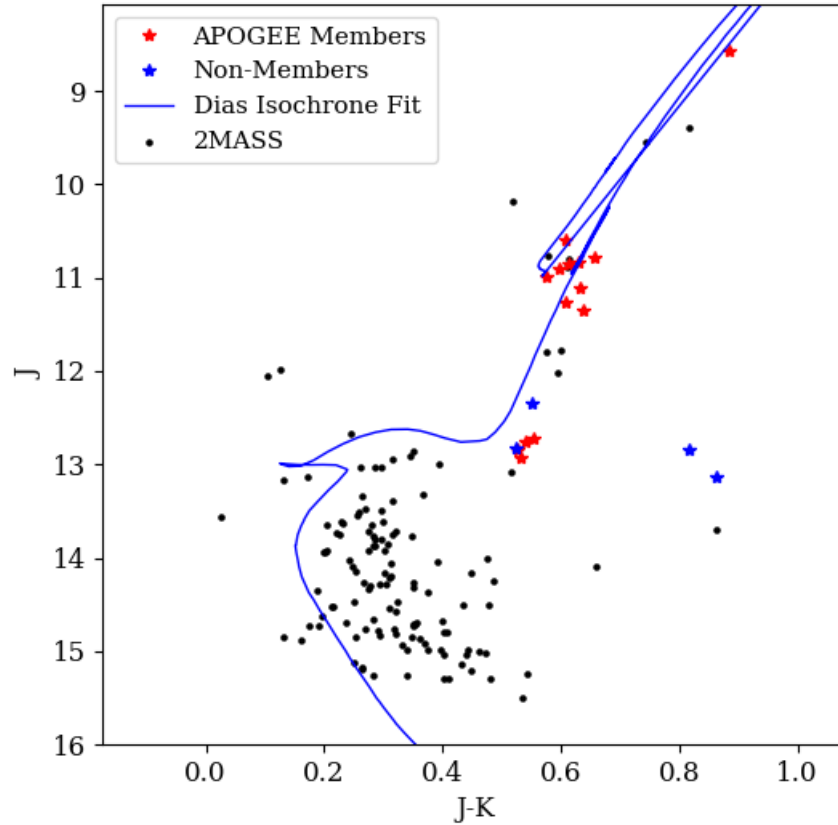


Figure 4.4: The CMD for NGC 2420, with APOGEE member stars shown in red and non-members shown in blue, plotted over the cluster stars. An isochrone fit based on catalog parameters from Dias et al. (2002) is also shown.

### 4.3 Determination of Galactic Abundance Gradients

A “very high reliability” criterion is adopted for a cluster to be included in our sample: 5 or more likely member stars, as determined above. This resulted in a total sample of 645 member stars in 49 clusters used for the analysis of galactic abundance gradients. The full cluster sample with the number of stars in each cluster and their derived and catalog parameters is presented in Appendix A.

The final value for  $[\text{Fe}/\text{H}]$  used for computing metallicity gradients is taken to be the mean metallicity of the likely members (here, we use the calibrated  $[\text{Fe}/\text{H}]$ , reported as ‘FE\_H’ in DR14). The uncertainty on this value is taken to be the standard deviation of their metallicities, meaning any abnormal internal dispersion will be reflected as a larger uncertainty. The quadrature of the  $[\text{Fe}/\text{H}]$  uncertainties reported from the data reduction pipeline was also considered for use as the reported uncertainty, however it was determined that the low uncertainties reported for individual stars resulted in an under-estimation of the true uncertainty in the metallicity of the cluster.

Using catalog values (Dias et al. 2002) for the distance and age of each cluster, we are able to perform any number of measurements of the abundance gradient for various sub-populations of different ages or distances from the disc. For this analysis, we assume a solar distance to the galactic center of 8 kpc.

### 4.3.1 Error Analysis

The scatter in the abundance gradients necessitates some reliable determination of the uncertainty in any quoted gradient. A bootstrap routine is used to estimate the error in gradients. The gradient is determined  $100 \times N$  times, where  $N$  is the number of clusters the line is being fit to (unless the number is very low, as is the case for our “old” cluster sample, in which case a minimum of 1000 runs was required), each time using a randomly determined  $[\text{Fe}/\text{H}]$  for each cluster, sampled from a standard normal distribution within its uncertainty. The mean of the resulting sample of  $100N$  gradients is adopted, and the standard deviation is taken as the uncertainty.

# Chapter 5

## Results & Discussion

### 5.1 Galactic Abundance Gradients

With a sample of 645 stars in 49 open clusters, Figure 5.1 represents one of the most sought after measurements in modern astronomy: the largest ever measurement of the galactic abundance gradient using a uniform sample.

The sample covers the disc from  $R_{GC} \approx 7.5$  to 12.5 kpc, with no major gaps. The majority of the sample is near the disc ( $z < 0.1$  kpc). The sample is also fairly young, with more than half being less than 1 Gyr old.

The overall gradient, with no cuts to age or z-height, is found to be  $-0.059 \pm 0.006$  dex  $\text{kpc}^{-1}$  (Figure 5.1 (a)). Unless we remove the “odd-ball” cluster, NGC 6791, which is commonly done in the literature, in which case we find a roughly 10% shallower gradient of  $-0.053 \pm 0.006$  dex  $\text{kpc}^{-1}$  (Figure 5.1 (b)). NGC 6791 is omitted from the remainder of the analysis due to its propensity to skew results.

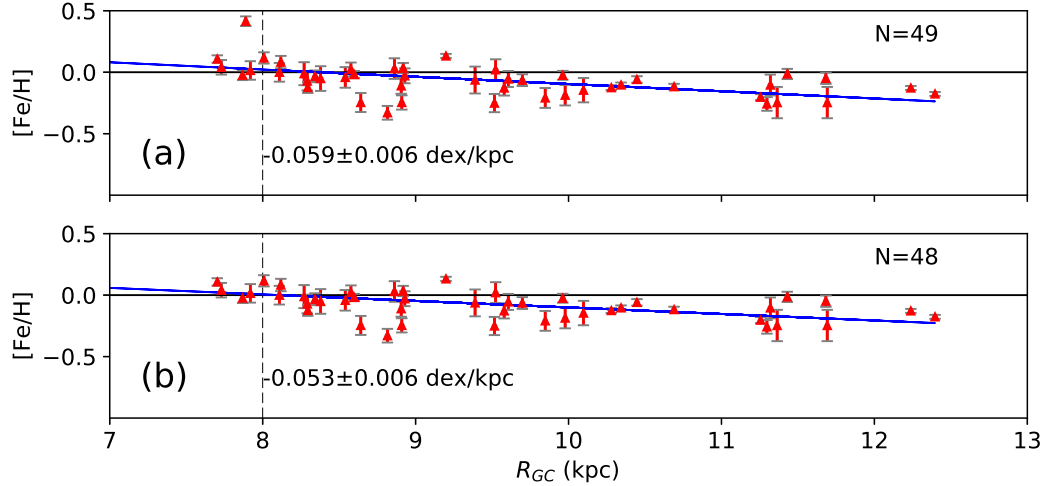


Figure 5.1: The very high reliability abundance gradients using APOGEE clusters. (a) shows the entire sample, while (b) shows the sample with the very metal-rich “odd-ball” NGC 6791 removed.

We can readily compare this result to Table 3.1. Our result is in agreement with 4 out of the 7 studies. However, it is in good agreement with 2 studies worth emphasizing: Friel et al. 2002 and Reddy et al. 2016 both had very large uniform samples (24 and 28 respectively) in addition to the literature. Some conclusions might be drawn from the good agreement of our own entirely uniform measurement closely with these studies, but not necessarily the studies with a larger percentage of literature compiled clusters. Reddy et al. is also the most recent measurement of this gradient.

### 5.1.1 Is The Thick Disk Real?: The $Z_{GC}$ Divided Sample

Figure 5.2 shows a breakdown of gradients in different  $z$ -height bins. The bins were chosen so that our sample showed roughly equal numbers in each bin. No detailed studies with  $z$ -height studied in bins exist in the literature (some studies of a continuous gradient exist, but that is unhelpful here, and in fact somewhat controversial (Carraro et al. 1998)), so

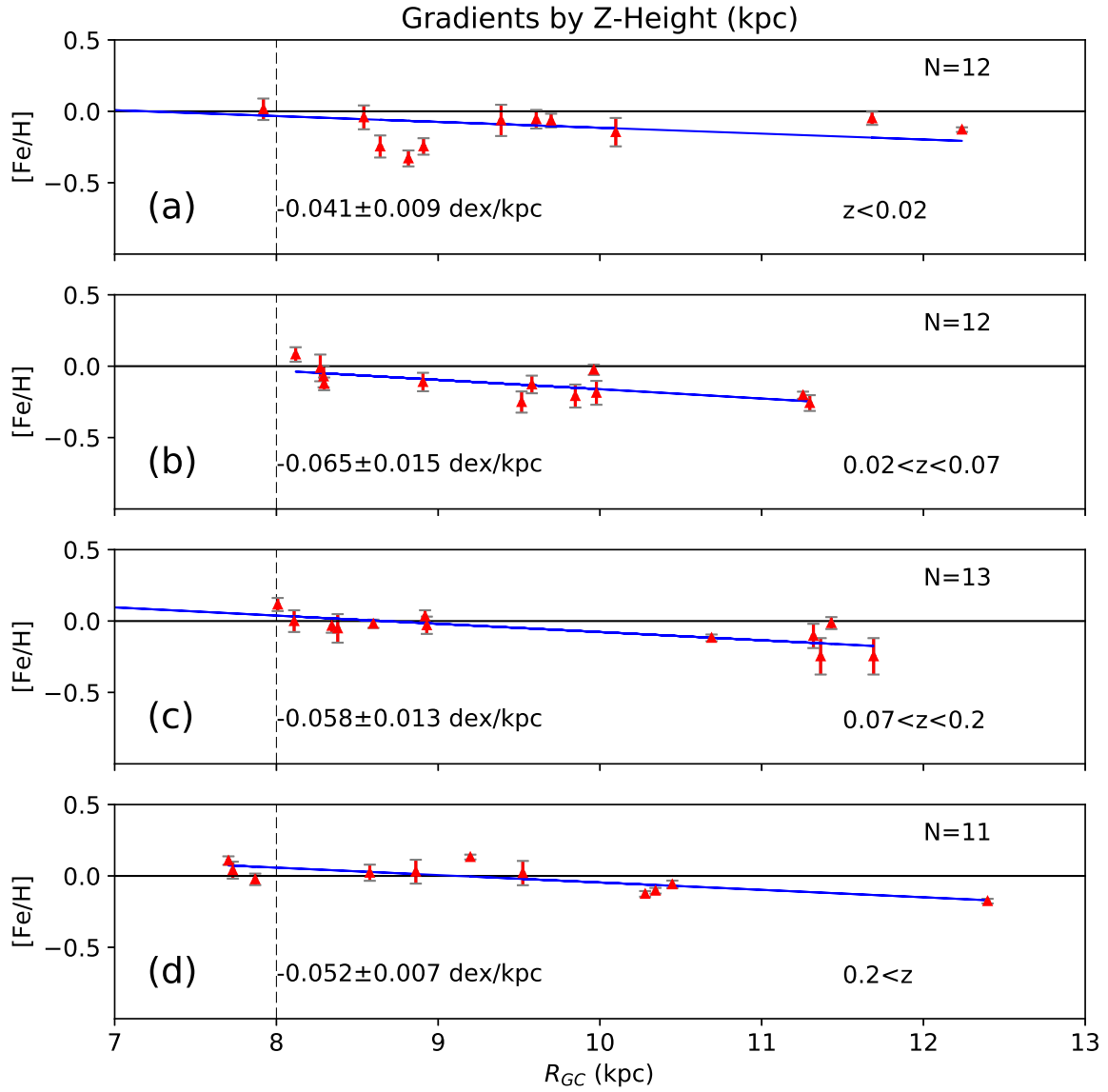


Figure 5.2: The galactic abundance gradient within various slices of the disc, chosen so that each bin includes approximately equal numbers of clusters.  $R_{GC}$  and  $z$  are in kpc.

there is no ideal choice for bin size. The equal bin sizes at least ensure that any trends are real and not the result of poor sampling.

No work has been done comparing radial abundance gradients as a function of  $z$ -height, although it is predicted and reported by modelers. Using equal-sample-size bins produces potentially odd cuts in  $z$ , so the close agreement of the middle 2 bins, (b) & (c), may indicate those populations should be considered together. Whether they are considered together or not, there is certainly a trend of increasingly steep gradients with  $z$ . The slope in the inner disc is apparently relatively shallow.

It is difficult to compare to the models of Minchev et al. (2014) (Figure 3.3), because their  $z$ -bins are much larger, with the 2nd bin beginning after our last bin. But even if we consider only general trends, or if we consider our “low  $z$ ” and “higher  $z$ ” sample, they trend in the opposite direction of Minchev et al. (2014). It is prudent then to discuss a limitation of this observational sample: clusters change height during their orbit of the galactic center. The heights reported in Dias et al. (2002) are current, observed heights, which is perfectly reasonable for an observation based catalog. However, to compare accurately to the models, some absolute measurement of  $z$  over the course of the cluster orbit needs to be determined, potentially the height at which the cluster formed, or else the maximum height it will attain. This is discussed in §6.3.

### **5.1.2 The Gradient Evolution?: The Age Divided Sample**

Figure 5.3 shows a breakdown of gradients in different age bins. The age bins were chosen to match previous work as closely as possible, however the lower limit on the oldest bin

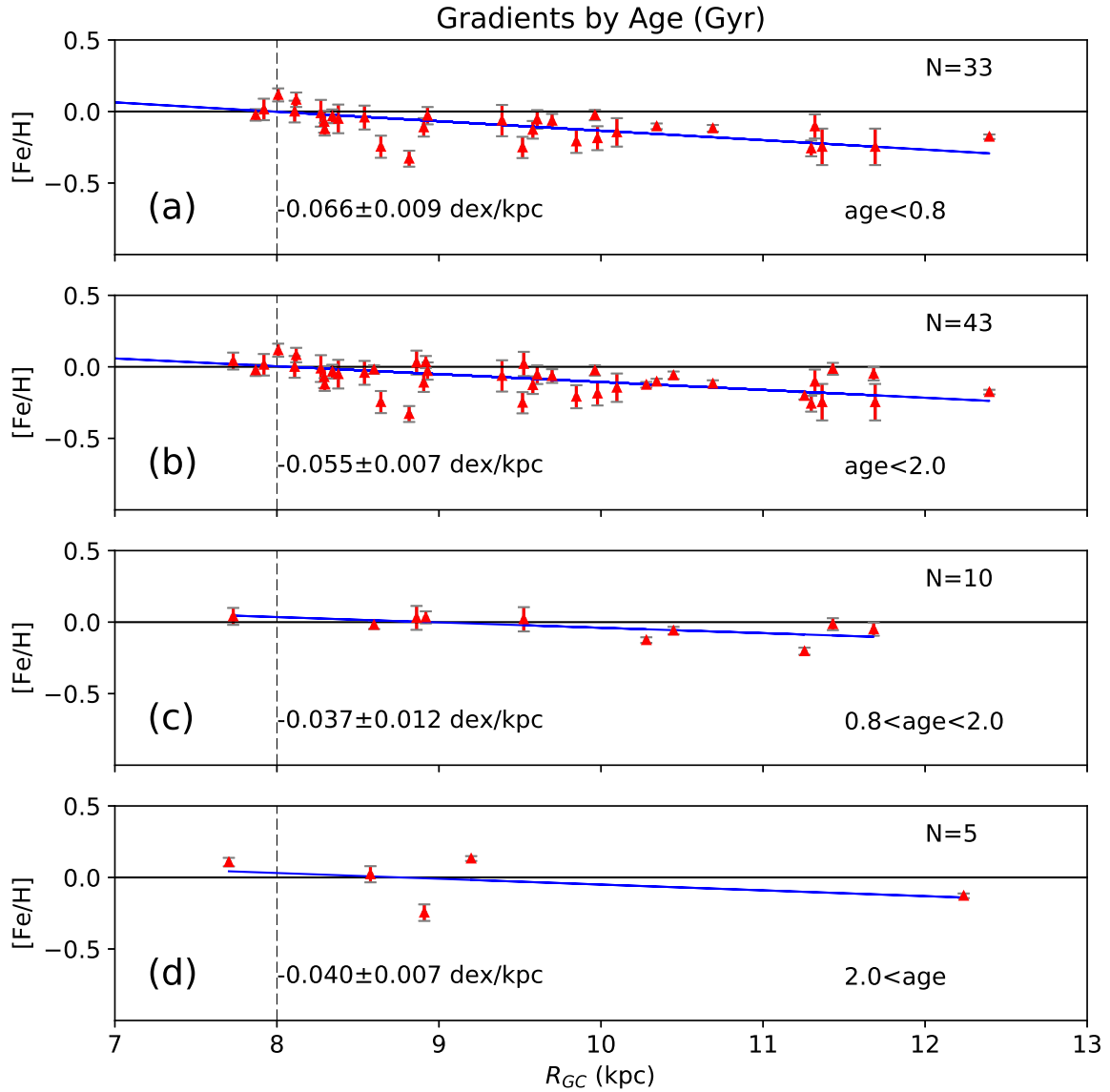


Figure 5.3: The galactic abundance gradient for clusters of varying age, chosen so that each bin includes approximately equal numbers of clusters. The age range is given in Gyr in the bottom right, and  $R_{GC}$  is in kpc.

was lowered to 2 Gyr (from the more common 4 Gyr adopted in the literature), so the sample included more than 2 clusters. 2 “young” age bins are presented since Yong et al. (2012) used an older upper limit for their “young” sample. Panel (a) shows the commonly used age bins, while (b) shows the bin used by Yong et al. (2012).

The age divided sample can be compared directly with previous work, given our care to keep the bins similar. A summary can be found in Table 5.1. Previous work from Yong et al. (2012) and Jacobson et al. (2011) found an increased spread in the data points with age, which we don’t necessarily see moving from the young sample to the middle-aged sample, but we may see moving from our middle-aged sample to our old sample. Jacobson et al. (2011), Friel & Janes (1993), and Carraro et al. (1998) consistently found an increasingly steep slope with age. Our results show the middle-age sample having a *less* steep slope than the young sample, although the two are indistinguishable within their uncertainties. The slope of our old sample is virtually identical to that of the middle-age sample.

Comparing to the galactic chemical evolution model of Minchev et al. (2014), we find somewhat close agreement with our results. The age bins used do not match those used in this study or any other referenced (see Table 5.1), however some of them are fairly close. The values reported are easily within the errors of this study, for all 3 age bins. Importantly, the “trend” with age in Minchev et al. (2014), considered for the other studies, matches well to this study.

Study	Young a<0.8	Middle-Age 0.8<a<4*	Old 4<a
Friel & Janes (1993)	-0.023	-0.053	-0.075
Carraro et al. (1998)	-0.06	-0.11	-0.12
Jacobson et al. (2011)	N/A	-0.083	-0.134
Minchev et al. (2014) <sup>+</sup>	-0.058	-0.048	-0.036
This Study	-0.066	-0.038	-0.040

Table 5.1: A summary of reported abundance gradients broken down by age bins. Only the 3 studies mentioned in §3.3 which reported gradients broken down by age are shown. Yong et al. (2012) is omitted because no numerical gradients are for their age-binned sample. The “Young”, “Middle-Age”, and “Old” labels are given, as well as the age ranges from the studies.

\* A reminder that the old sample presented in this work is  $> 2$  Gyr, not 4 Gyr.

<sup>+</sup> We include results from current galactic chemical evolution models as well. The youngest age bin given by the authors is  $a < 2$  Gyr, then  $2 < a < 4$ , which we use for the middle-age bin. An average of their older age bins is given for the old bin.

### 5.1.3 Discussion

These results present a clear departure from the literature. All of the observational samples previously seemed to suggest the existence of an increasingly steep gradient with age. We have found no evidence for this, and potential evidence for a trend in the opposite direction. Critically: this trend is seen in current models of galactic chemical evolution.

However, the studies compared to often had more clusters at lower and/or higher  $R_{GC}$  than our sample (for example, see Figure 3.4). They also tended to have many more clusters in their “old” samples, whereas our “old” sample is potentially unreliable. The results we present raise important questions, but will require careful follow up.

It is important to recognize the limitations of this study. The largest limitation is simply our sample size. While this is the largest sample of open clusters with *uniform* measurements of their chemical composition ever compiled, it is not large enough to

cover the entire disc, or to cover the oldest of the age bins considered densely enough to reliably measure a gradient, or to explore even older age bins (as both the models and other studies do).

The other large limitation is the use of catalog values for both age and  $R_{GC}$ . Some of the values from Dias et al. (2002) come from literature sources, others are derived by the authors, but as seen in Figure 4.4, they aren't necessarily reliable.

Both of these shortcomings will be addressed in future work (see Chapter 6).

# Chapter 6

## Future Work

### 6.1 Improve Isochrone Fitting

Distance to open clusters is a key underpinning of the gradients derived in this work. Distances used in this work come from the Dias catalog (Dias et al. 2002) and are derived from isochrone fitting. As mentioned in §1.5, blind (that is, uninformed by spectroscopic metallicity) isochrone fitting is subject to age-metallicity degeneracies. Fitting in a 4-dimensional space is also intrinsically difficult. The fitting problem generally involves minimizing some objective function which evaluates the fit of an isochrone model to some set of stars. With a large number of stars, and a discrete model (one defined by a series of points, with no simple functional representation), solving this problem in 4 dimensions can quickly become computationally difficult, without even overcoming the age-metallicity degeneracies!

Recently Correnti et al. (2016) developed a computationally efficient Bayesian method to fit isochrones to globular cluster CMDs. Their method uses a kernel-density-estimator

(KDE) routine to create a fiducial representation of the cluster and generate a functional representation. The resulting fiducial is then computationally trivial to compare to a suite of isochrones, allowing for a Bayesian estimation of probability density in the 4-D space.

The approach of Correnti et al. uses a uniform prior in each of the 4 dimensions. We believe this could be greatly improved upon for any cluster with APOGEE stars. The metallicity uncertainties from Correnti et al. are nearly a full order of magnitude greater than APOGEE uncertainties on metallicity. This means we can either provide excellent priors for the analysis of open clusters, or completely eliminate a dimension in the fitting process.

It is worth addressing that open clusters suffer from a problem unique from globular clusters: field star contamination. Due to their location in the galactic disc (as opposed to globular clusters, located high above the disc), open cluster fields generally contain many stars along the line of sight that are not part of the cluster. When generating a fiducial representation using a KDE, these stars may cause a problem.

The other large problem this research will face is data quality. The method of Correnti et al. relied on high quality Hubble Space Telescope (HST) photometry. This data is not generally available for open clusters. 2MASS photometry, while available for the whole sky, often only captures the brightest parts of open clusters, and even then is subject to significant uncertainties. Deeper infrared surveys exist however, and more recently the PanSTARRS (Chambers et al. 2016) survey promises to provide optical photometry for stars down to visual magnitudes of  $\approx 21$ . This very faint magnitude limit will allow us to capture the majority of most open clusters in optical wavelengths, with low uncertainties.

The combination of APOGEE priors and very faint PanSTARRS photometry make this avenue very promising. We expect to obtain not only far more accurate distances and ages, but *uniform* distances and ages for our entire open cluster sample. Additionally, the Bayesian analysis may allow us to determine a membership probability for any star based on its location in the CMD and calculate a probability density function from the fit parameters (this is by no means necessary, but may further constrain membership analysis and make other measurements more accurate).

## 6.2 The *Gaia* Survey

The *Gaia* survey is a space based European Space Agency (ESA) mission. It will provide proper motion analysis for stars as far as 10 kpc, and distances for stars as far as 1 kpc. We will therefore have a very accurate calibration for the method described above, for the nearby clusters.

Proper motion is a measure of a star’s lateral (perpendicular to line of sight) movement on the sky. Similar to RV, all the star’s in a cluster will move with similar proper motions (because they are gravitationally bound). We are therefore able to extend the 1-dimensional RV and [Fe/H] analysis of §4.2.3.1 to 2 dimensions, the 2 dimensions of motion on the sky. The analysis is nearly identical (a 2D Gaussian kernel smoothing routine is applied and a 2D Gaussian is fit), and we have already tested it successfully for the nearby cluster NGC 2682. Unfortunately, the test was for only a dozen or so stars, and other clusters had only a handful. For the 2-dimensional analysis to yield a strong “peak” (representing the cluster), a dozen stars is close to the minimum required.

With *Gaia*, we can expect dozens of stars in each of hundreds of open clusters, as far as 10 kpc away. This will allow us to clearly identify the cluster behavior from proper motion analysis, and determine proper motion membership probabilities for any APOGEE star in that field. Thus, we can potentially establish a single APOGEE star as a cluster member, without losing confidence in that membership probability. The sample presented in this work was 49 open clusters. The targeted open cluster sample was close to 400, but this includes small clusters where only 1 star could be observed. The addition of *Gaia* data could then increase our sample by up to 8-fold.

### 6.3 Improved Z-Height Measurements

The reported analysis with Z-height is based on the current positions of these clusters, as discussed in §5.1. With the addition of *Gaia*, and the improved distance measurements, we will be able to calculate the full 6-D position and velocity phase-space for the cluster sample. With the addition of a galactic gravitational potential model, orbits for each cluster can be predicted into the future, or integrated into the past. This will allow us to compare to models far more accurately than currently possibly.

# Appendix A

## The Cluster Sample

Table A.1: The full sample of very high confidence clusters. The number of APOGEE stars and their mean [Fe/H] are given, as well as values used for gradient analysis from Dias et al. (2002).

\* indicates a cluster with age  $< 0.01$  Gyr, possibly estimated at as low as 1 Myr

Name	# Stars	[Fe/H] (dex)	$\sigma$ [Fe/H] (dex)	RV (km s <sup>-1</sup> )	$\sigma$ RV (km s <sup>-1</sup> )	$Z_{GC}$ (kpc)	$R_{GC}$ (kpc)	Age (Gyr)
Alessi 20	6	-0.12	0.04	-73.0	3.0	0.039	8.3	0.00*
FSR 0494	7	-0.01	0.04	-62.8	1.6	0.091	11.4	2.00
NGC 129	5	-0.03	0.06	-57.9	5.4	0.072	8.9	0.08
NGC 188	6	0.13	0.02	-41.8	1.6	0.780	9.2	4.29
IC 166	19	-0.05	0.05	-40.4	1.5	0.016	11.7	1.00
Czernik 6	5	-0.19	0.08	-51.1	4.1	0.050	10.0	0.01
Berkeley 66	7	-0.13	0.02	-50.0	0.4	0.019	12.2	3.98
NGC 1245	25	-0.06	0.03	-29.3	0.8	0.437	10.4	1.07
Melotte 22	54	0.08	0.05	5.7	1.1	0.053	8.1	0.14
King 7	6	-0.03	0.04	-10.1	1.4	0.039	10.0	0.66

NGC 1545	7	-0.25	0.08	-16.9	3.9	0.002	8.6	0.28
Platais 4	8	-0.01	0.09	-6.5	3.6	0.052	8.3	0.10
NGC 1798	13	-0.18	0.02	2.5	0.9	0.386	12.4	0.79
Czernik 20	14	-0.10	0.08	3.9	4.0	0.085	11.3	0.01
Berkeley 17	6	-0.12	0.02	-73.3	0.2	0.172	10.7	0.00*
NGC 1912	7	-0.06	0.11	10.6	3.0	0.017	9.4	0.32
Collinder 69	18	-0.05	0.10	28.3	3.5	0.083	8.4	0.01
Koposov 36	5	-0.06	0.05	19.5	5.1	0.012	9.7	0.22
Sigma Orionis	11	-0.03	0.05	30.0	0.9	0.119	8.3	0.01
FSR 0816	5	-0.15	0.10	-21.5	2.8	0.007	10.1	0.56
Teutsch 1	5	-0.25	0.13	-16.1	2.4	0.071	11.4	0.07
Koposov 27	5	-0.25	0.13	-16.1	2.4	0.078	11.7	0.45
Berkeley 71	9	-0.20	0.02	-9.7	0.3	0.051	11.3	1.00
Teutsch 51	8	-0.26	0.06	16.9	1.4	0.028	11.3	0.79
NGC 2168	9	-0.11	0.06	-7.4	2.7	0.035	8.9	0.18
NGC 2175	5	-0.06	0.06	-1.3	3.4	0.014	9.6	0.01
NGC 2244	5	-0.25	0.07	80.3	4.4	0.060	9.5	0.00*
NGC 2240	5	0.02	0.08	-9.9	3.2	0.318	9.5	1.58
NGC 2252	6	-0.33	0.06	70.4	3.8	0.020	8.8	0.69
Collinder 104	6	-0.21	0.08	60.3	3.8	0.039	9.8	0.32
Collinder 106	11	-0.25	0.06	60.7	3.2	0.008	8.9	7.94
Collinder 107	8	-0.13	0.06	33.1	3.9	0.027	9.6	0.01
NGC 2413	7	-0.07	0.08	95.7	4.2	0.022	8.3	0.29
Melotte 71	5	-0.10	0.02	50.7	0.6	0.247	10.3	0.23

NGC 2420	14	-0.13	0.02	74.2	0.5	0.833	10.3	2.00
NGC 2682	158	0.02	0.06	33.9	1.0	0.427	8.6	2.82
Melotte 111	9	0.12	0.05	-3.6	3.8	0.095	8.0	0.45
Dol Dzim 5	5	0.04	0.06	4.4	3.2	0.624	7.7	2.00
Teutsch 14a	5	0.31	0.05	-30.0	2.8	0.001	6.3	0.10
NGC 6705	11	0.17	0.03	35.1	0.9	0.091	6.4	0.25
NGC 6791	23	0.41	0.04	-47.0	1.4	0.952	7.9	8.32
NGC 6811	6	-0.02	0.04	6.5	1.7	0.253	7.9	0.63
NGC 6819	36	0.11	0.03	2.5	1.6	0.371	7.7	2.40
Roslund 6	5	0.01	0.08	-18.3	3.9	0.002	7.9	0.30
Berkeley 53	9	-0.02	0.03	-36.0	1.1	0.200	8.6	1.23
IC 5146	6	-0.00	0.08	-8.2	2.9	0.082	8.1	0.00*
NGC 7175	7	-0.04	0.08	-76.1	4.2	0.003	8.5	0.25
vdBergh 152	5	0.03	0.08	-10.1	4.6	0.387	8.9	1.97
NGC 7789	18	0.03	0.04	-54.9	0.7	0.168	8.9	1.41

---

# Bibliography

- Abolfathi, B., Aguado, D. S., Aguilar, G., Allende Prieto, C., Almeida, A., Tasnim Ananna, T., Anders, F., Anderson, S. F., Andrews, B. H., Anguiano, B., & et al. 2017, ArXiv e-prints
- Andrews, B. H., Weinberg, D. H., Schönrich, R., & Johnson, J. A. 2017, *The Astrophysical Journal*, 835, 224
- Bensby, T., Feltzing, S., Lundström, I., & Ilyin, I. 2005, *Astronomy and Astrophysics*, 433, 185
- Bland-Hawthorn, J. & Gerhard, O. 2016, *The Annual Review of Astronomy and Astrophysics*, 54, 529
- Blanton, M. R., Bershady, M. A., Abolfathi, B., Albareti, F. D., Allende Prieto, C., Almeida, A., Alonso-García, J., Anders, F., Anderson, S. F., Andrews, B., & et al. 2017, *The Astronomical Journal*, 154, 28
- Bovy, J., Rix, H.-W., & Hogg, D. W. 2012a, *The Astrophysical Journal*, 751, 131
- Bovy, J., Rix, H.-W., Liu, C., Hogg, D. W., Beers, T. C., & Lee, Y. S. 2012b, *The Astrophysical Journal*, 753, 148
- Burstein, D. 1979, *The Astrophysical Journal*, 234, 829
- Carraro, G., Ng, Y. K., & Portinari, L. 1998, *Monthly Notices of the Royal Astronomy Society*, 296, 1045
- Chambers, K. C., Magnier, E. A., Metcalfe, N., Flewelling, H. A., Huber, M. E., Waters, C. Z., Denneau, L., Draper, P. W., Farrow, D., Finkbeiner, D. P., Holmberg, C., Koppenhoefer, J., Price, P. A., Saglia, R. P., Schlafly, E. F., Smartt, S. J., Sweeney, W., Wainscoat, R. J., Burgett, W. S., Grav, T., Heasley, J. N., Hodapp, K. W., Jedicke, R., Kaiser, N., Kudritzki, R.-P., Luppino, G. A., Lupton, R. H., Monet, D. G., Morgan, J. S., Onaka, P. M., Stubbs, C. W., Tonry, J. L., Banados, E., Bell, E. F., Bender, R., Bernard, E. J., Botticella, M. T., Casertano, S., Chastel, S., Chen, W.-P., Chen, X., Cole, S., Deacon, N., Frenk, C., Fitzsimmons, A., Gezari, S., Goessl, C., Goggia, T., Goldman, B., Grebel, E. K., Hambly, N. C., Hasinger, G., Heavens, A. F., Heckman, T. M., Henderson, R., Henning, T., Holman, M., Hopp, U., Ip, W.-H., Isani, S., Keyes, C. D., Koekemoer, A., Kotak, R., Long, K. S., Lucey, J. R., Liu, M., Martin, N. F.,

- McLean, B., Morganson, E., Murphy, D. N. A., Nieto-Santisteban, M. A., Norberg, P., Peacock, J. A., Pier, E. A., Postman, M., Primak, N., Rae, C., Rest, A., Riess, A., Riffeser, A., Rix, H. W., Roser, S., Schilbach, E., Schultz, A. S. B., Scolnic, D., Szalay, A., Seitz, S., Shiao, B., Small, E., Smith, K. W., Soderblom, D., Taylor, A. N., Thakar, A. R., Thiel, J., Thilker, D., Urata, Y., Valenti, J., Walter, F., Watters, S. P., Werner, S., White, R., Wood-Vasey, W. M., & Wyse, R. 2016, ArXiv e-prints
- Correnti, M., Gennaro, M., Kalirai, J. S., Brown, T. M., & Calamida, A. 2016, *The Astrophysical Journal*, 823, 18
- Council, N., Sciences, D., Board, S., Astronomy, B., & Astrophysics, C. 2011, *New Worlds, New Horizons in Astronomy and Astrophysics* (National Academies Press)
- Cutri, R. M., Skrutskie, M. F., van Dyk, S., Beichman, C. A., Carpenter, J. M., Chester, T., Cambresy, L., Evans, T., Fowler, J., Gizis, J., Howard, E., Huchra, J., Jarrett, T., Kopan, E. L., Kirkpatrick, J. D., Light, R. M., Marsh, K. A., McCallon, H., Schneider, S., Stiening, R., Sykes, M., Weinberg, M., Wheaton, W. A., Wheelock, S., & Zacarias, N. 2003, 2MASS All Sky Catalog of point sources.
- de Vaucouleurs, G. 1959, *Handbuch der Physik*, 53, 311
- Dias, W. S., Alessi, B. S., Moitinho, A., & Lépine, J. R. D. 2002, *Astronomy and Astrophysics*, 389, 871
- Donati, P., Bragaglia, A., Carretta, E., D’Orazi, V., Tosi, M., Cusano, F., & Carini, R. 2015, *Monthly Notices of the Royal Astronomy Society*, 453, 4185
- Eisenstein, D. J., Weinberg, D. H., Agol, E., Aihara, H., Allende Prieto, C., Anderson, S. F., Arns, J. A., Aubourg, É., Bailey, S., Balbinot, E., & et al. 2011, *The Astronomical Journal*, 142, 72
- Friel, E. D. 1995, *The Annual Review of Astronomy and Astrophysics*, 33, 381
- Friel, E. D. & Janes, K. A. 1993, *Astronomy and Astrophysics*, 267, 75
- Friel, E. D., Janes, K. A., Tavares, M., Scott, J., Katsanis, R., Lotz, J., Hong, L., & Miller, N. 2002, *The Astronomical Journal*, 124, 2693
- Frinchaboy, P., Zasowski, G., Jackson, K., Johnson, J. A., Majewski, S. R., Shetrone, M., Rocha, A., & SDSS-III Collaboration. 2010, in JENAM 2010, Joint European and National Astronomy Meeting, 136
- García Pérez, A. E., Allende Prieto, C., Holtzman, J. A., Shetrone, M., Mészáros, S., Bizyaev, D., Carrera, R., Cunha, K., García-Hernández, D. A., Johnson, J. A., Majewski, S. R., Nidever, D. L., Schiavon, R. P., Shane, N., Smith, V. V., Sobek, J., Troup, N., Zamora, O., Weinberg, D. H., Bovy, J., Eisenstein, D. J., Feuillet, D., Frinchaboy, P. M., Hayden, M. R., Hearty, F. R., Nguyen, D. C., O’Connell, R. W., Pinsonneault, M. H., Wilson, J. C., & Zasowski, G. 2016, *The Astronomical Journal*, 151, 144

- Gilmore, G. & Reid, N. 1983, *Monthly Notices of the Royal Astronomy Society*, 202, 1025
- Gunn, J. E., Siegmund, W. A., Mannery, E. J., Owen, R. E., Hull, C. L., Leger, R. F., Carey, L. N., Knapp, G. R., York, D. G., Boroski, W. N., Kent, S. M., Lupton, R. H., Rockosi, C. M., Evans, M. L., Waddell, P., Anderson, J. E., Annis, J., Barentine, J. C., Bartoszek, L. M., Bastian, S., Bracker, S. B., Brewington, H. J., Briegel, C. I., Brinkmann, J., Brown, Y. J., Carr, M. A., Czarapata, P. C., Drennan, C. C., Dombeck, T., Federwitz, G. R., Gillespie, B. A., Gonzales, C., Hansen, S. U., Harvanek, M., Hayes, J., Jordan, W., Kinney, E., Klaene, M., Kleinman, S. J., Kron, R. G., Kresinski, J., Lee, G., Limmongkol, S., Lindenmeyer, C. W., Long, D. C., Loomis, C. L., McGehee, P. M., Mantsch, P. M., Neilsen, Jr., E. H., Neswold, R. M., Newman, P. R., Nitta, A., Peoples, Jr., J., Pier, J. R., Prieto, P. S., Prosapio, A., Rivetta, C., Schneider, D. P., Snedden, S., & Wang, S.-i. 2006, *The Astronomical Journal*, 131, 2332
- Jacobson, H. R., Pilachowski, C. A., & Friel, E. D. 2011, *The Astronomical Journal*, 142, 59
- Kubryk, M., Prantzos, N., & Athanassoula, E. 2015, *Astronomy and Astrophysics*, 580, A127
- Magrini, L., Randich, S., Donati, P., Bragaglia, A., Adibekyan, V., Romano, D., Smiljanic, R., Blanco-Cuaresma, S., Tautvaišienė, G., Friel, E., Overbeek, J., Jacobson, H., Cantat-Gaudin, T., Vallenari, A., Sordo, R., Pancino, E., Geisler, D., San Roman, I., Villanova, S., Casey, A., Hourihane, A., Worley, C. C., Francois, P., Gilmore, G., Bensby, T., Flaccomio, E., Korn, A. J., Recio-Blanco, A., Carraro, G., Costado, M. T., Franciosini, E., Heiter, U., Jofré, P., Lardo, C., de Laverny, P., Monaco, L., Morbidelli, L., Sacco, G., Sousa, S. G., & Zaggia, S. 2015, *Astronomy and Astrophysics*, 580, A85
- Majewski, S. R., Schiavon, R. P., Frinchaboy, P. M., Allende Prieto, C., Barkhouser, R., Bizyaev, D., Blank, B., Brunner, S., Burton, A., Carrera, R., Chojnowski, S. D., Cunha, K., Epstein, C., Fitzgerald, G., García Pérez, A. E., Hearty, F. R., Henderson, C., Holtzman, J. A., Johnson, J. A., Lam, C. R., Lawler, J. E., Maseman, P., Mészáros, S., Nelson, M., Nguyen, D. C., Nidever, D. L., Pinsonneault, M., Shetrone, M., Smee, S., Smith, V. V., Stolberg, T., Skrutskie, M. F., Walker, E., Wilson, J. C., Zasowski, G., Anders, F., Basu, S., Beland, S., Blanton, M. R., Bovy, J., Brownstein, J. R., Carlberg, J., Chaplin, W., Chiappini, C., Eisenstein, D. J., Elsworth, Y., Feuillet, D., Fleming, S. W., Galbraith-Frew, J., García, R. A., García-Hernández, D. A., Gillespie, B. A., Girardi, L., Gunn, J. E., Hasselquist, S., Hayden, M. R., Hekker, S., Ivans, I., Kinemuchi, K., Klaene, M., Mahadevan, S., Mathur, S., Mosser, B., Muna, D., Munn, J. A., Nichol, R. C., O’Connell, R. W., Parejko, J. K., Robin, A. C., Rocha-Pinto, H., Schultheis, M., Serenelli, A. M., Shane, N., Silva Aguirre, V., Sobeck, J. S., Thompson, B., Troup, N. W., Weinberg, D. H., & Zamora, O. 2017, *The Astronomical Journal*, 154, 94

- Majewski, S. R., Zasowski, G., & Nidever, D. L. 2011, *The Astrophysical Journal*, 739, 25
- Marigo, P., Girardi, L., Bressan, A., Groenewegen, M. A. T., Silva, L., & Granato, G. L. 2008, *Astronomy and Astrophysics*, 482, 883
- Minchev, I., Chiappini, C., & Martig, M. 2013, *Astronomy and Astrophysics*, 558, A9
- . 2014, *Astronomy and Astrophysics*, 572, A92
- Netopil, M., Paunzen, E., Heiter, U., & Soubiran, C. 2016, *Astronomy and Astrophysics*, 585, A150
- Nidever, D. L., Bovy, J., Bird, J. C., Andrews, B. H., Hayden, M., Holtzman, J., Majewski, S. R., Smith, V., Robin, A. C., García Pérez, A. E., Cunha, K., Allende Prieto, C., Zasowski, G., Schiavon, R. P., Johnson, J. A., Weinberg, D. H., Feuillet, D., Schneider, D. P., Shetrone, M., Sobek, J., García-Hernández, D. A., Zamora, O., Rix, H.-W., Beers, T. C., Wilson, J. C., O’Connell, R. W., Minchev, I., Chiappini, C., Anders, F., Bizyaev, D., Brewington, H., Ebelke, G., Frinchaboy, P. M., Ge, J., Kinemuchi, K., Malanushenko, E., Malanushenko, V., Marchante, M., Mészáros, S., Oravetz, D., Pan, K., Simmons, A., & Skrutskie, M. F. 2014, *The Astrophysical Journal*, 796, 38
- Pancino, E., Carrera, R., Rossetti, E., & Gallart, C. 2010, *Astronomy and Astrophysics*, 511, A56
- Reddy, A. B. S., Lambert, D. L., & Giridhar, S. 2016, *Monthly Notices of the Royal Astronomy Society*, 463, 4366
- Rodrigo, C., S. E. B. A. 1999, *The SVO Filter Profile Service*
- Trumpler, R. J. 1930, *Lick Observatory Bulletin*, 14, 154
- Wright, E. L., Eisenhardt, P. R. M., Mainzer, A. K., Ressler, M. E., Cutri, R. M., Jarrett, T., Kirkpatrick, J. D., Padgett, D., McMillan, R. S., Skrutskie, M., Stanford, S. A., Cohen, M., Walker, R. G., Mather, J. C., Leisawitz, D., Gautier, III, T. N., McLean, I., Benford, D., Lonsdale, C. J., Blain, A., Mendez, B., Irace, W. R., Duval, V., Liu, F., Royer, D., Heinrichsen, I., Howard, J., Shannon, M., Kendall, M., Walsh, A. L., Larsen, M., Cardon, J. G., Schick, S., Schwalm, M., Abid, M., Fabinsky, B., Naes, L., & Tsai, C.-W. 2010, *The Astronomical Journal*, 140, 1868
- Yong, D., Carney, B. W., & Friel, E. D. 2012, *The Astronomical Journal*, 144, 95

## VITA

Personal Background	John Richard Donor III Bedford, TX Son of John and Amy Donor Married Rachel Christine Du Frane, June 17, 2017
Education	Diploma, Lawrence D. Bell High School, Hurst, TX, 2010 Bachelor of Arts, Physics, Austin College, Sherman, TX, 2010
Experience	Summer research assistant, Austin College, Sherman, TX, 2013 Teaching assistantship, Texas Christian University, Fort Worth, 2014-2017
Professional Memberships	American Astronomical Society

## ABSTRACT

### A UNIFORM MEASUREMENT OF THE GALACTIC ABUNDANCE GRADIENT

by John R Donor III, 2017  
Department of Physics and Astronomy  
Texas Christian University

Peter M. Frinchaboy III, Associate Professor of Physics

Despite living inside the Milky Way, we do not know well basic quantities such as its detailed chemical makeup at the level needed to fundamentally tie the Milky Way to studies of evolution in other galaxies. One key observable is the radial chemical abundance gradient. Open star clusters provide an age datable sample by which to measure this gradient. This measurement has previously been made using a diverse and regularly conflicting compilation of clusters from various literature studies. We present the first measurement using a large (645 stars in 49 open clusters), *uniform* sample of open clusters abundances. Our measurements show a general agreement with recent studies of the overall metallicity gradient, with a measured  $\Delta [\text{Fe}/\text{H}]/\Delta R_{GC}$  of  $-0.053 \pm 0.006 \text{ dex kpc}^{-1}$ . We also explore trends with  $Z_{GC}$  and cluster age, and find significant departure from the observed trends as the sample age increases.